J. Fluid Mech. (1994), *vol.* 278, *pp.* 363–390

Unsteady flow near a moving cylinder

By A. P. DOWLING

Cambridge University Engineering Department, Trumpington Street, Cambridge CB2 1PZ, UK

(Received 11 June 1992 and in revised form 10 June 1994)

General representations are derived for both the velocity potential and the surface pressure fluctuations induced by an arbitrary distribution of vorticity near a manoeuvring cylinder. The cylinder is inextensible and in unsteady motion. Its axis may be slightly curved, with radius of curvature large in comparison with the cylinder radius.

Two model problems are considered in detail to investigate the effect of lateral displacements of a cylinder with an established boundary layer. The boundary layer on the flexible cylinder is found to be shed once the lateral displacement of the cylinder axis exceeds the boundary-layer thickness. The unsteady pressures generated by this vortex shedding are investigated.

1. Introduction

The forces acting on slender fish and long, flexible cylinders have been studied extensively (see, for example, Taylor 1952; Lighthill 1960 and Paidoussis 1973). One particular application is to towed instrumentation packages in the form of long flexible cylinders which are used to detect and analyse acoustic signals in the ocean (Kennedy 1980; Dowling 1988). The cylinder is usually neutrally buoyant and contains an axially distributed sonar array. This cylinder is sometimes referred to as an acoustic 'streamer' or 'array'. Under constant towing conditions, the towed array is straight and parallel. However, changes in ship heading and speed cause transverse motion of the array, deforming it from a straight cylinder. Array deflection can also be produced by ocean currents. It may be possible to extend the operating range of a towed array into this deformed case, but to do so more details of the unsteady flow near a manoeuvring cylinder are needed.

Consider a cylinder in motion with an arbitrary unsteady velocity, $U(s,t)$, where $U(s,t)$ is a gradually varying function of arclength s along the cylinder. This leads to deflections of the cylinder, with an axial lengthscale much larger than the cylinder radius a. It is convenient to decompose the fluid velocity due to the cylinder motion into the sum of an irrotational component and that induced by vorticity.

The irrotational flow produced by an arbitrary unsteady motion of a cylinder with a slightly curved axis is investigated in §2. The method of matched asymptotic expansions is used to determine the near-field velocity potential correct to order a/R_c, where R_c is the radius of curvature of the cylinder axis.

The effect of vorticity is considered in §3. Möhring (1978) introduced a vector Green function to obtain a convenient description of the distant sound generated by vorticity. We apply the same idea to the incompressible near field induced by vorticity. It enables us to determine a general expression for the velocity potential produced outside the vortical region by an arbitrary three-dimensional distribution of vorticity near a moving cylinder. This extends the classical result for the velocity potential due to a line

vortex parallel to a cylinder axis (see for example Batchelor 1967, p. 423) to three dimensions. Having determined the velocity potential, it is straightforward to calculate other flow parameters, like velocity and pressure.

The pressure field generated on the cylinder is of particular interest for the towed array geometry. Embedded transducers within the array measure the circumferentially averaged surface pressure. This information is then used to evaluate the axial-wavenumber decomposition of the measured pressure. We use our expression for the velocity potential to deduce a representation for the axial-wavenumber decomposition of the circumferentially averaged surface pressure, in terms of a weighted integral over the instantaneous vorticity fields (see (3.30)). Further simplification is possible when the vorticity is linear, so that it convects with the irrotational fluid velocity induced by the cylinder motion.

In §4 we illustrate how this representation theorem can be used by considering two simplified model problems. We wish to investigate the unsteady pressures generated when a cylinder with an established boundary layer undergoes lateral displacement. Only a very simple model of an element of boundary-layer turbulence is considered. It is modelled by a vortex ring of linear strength, which is initially coaxial with the cylinder. We find that transverse cylinder motion significantly distorts the vortex ring, and that vorticity is essentially shed from the cylinder once the displacement of the axis of the cylinder exceeds the initial ring diameter. This means that the boundary layer is continually being shed from a flexible cylinder undergoing lateral displacements. Whereas the boundary layer on a straight cylinder aligned with the flow grows with distance from its leading edge, we can expect the boundary layer on a flexible cylinder to be shed once the lateral displacement of the cylinder axis exceeds the boundary-layer thickness. Hence along a flexible cylinder the boundary layer will repeatedly grow and then be shed. The results of §3 are used to calculate the axial-wavenumber decomposition of the circumferentially averaged surface pressure induced by this shedding process.

2. Irrotational flow near a slightly curved cylinder

Consider the inextensible flexible cylinder illustrated in figure 1. We denote the position vector of the cylinder axis at arclength s and time t by $\boldsymbol{x}_c(s, t)$. The unit vector in the direction of the cylinder axis $\hat{\boldsymbol{s}}$, is then given by $\hat{\boldsymbol{s}} = \partial \boldsymbol{x}_c/\partial s|_t$ while the cylinder velocity, $\boldsymbol{U}(s, t)$, is denoted by $\boldsymbol{U} = \partial \boldsymbol{x}_c/\partial t|_s$. The inextensibility of the cylinder imposes a constraint on its velocity, which (see Batchelor 1967, p. 132) can be expressed as

$$\hat{\boldsymbol{s}} \cdot \partial \boldsymbol{U}/\partial s = 0. \tag{2.1}$$

The instantaneous curvature of the cylinder axis, $\boldsymbol{\rho}(s, t)$, is defined by $\boldsymbol{\rho}(s, t) = \partial \hat{\boldsymbol{s}}/\partial s|_t$. Since $\hat{\boldsymbol{s}}$ is a unit vector

$$\hat{\boldsymbol{s}} \cdot \boldsymbol{\rho} = \frac{1}{2} \frac{\partial}{\partial s} (\hat{\boldsymbol{s}} \cdot \hat{\boldsymbol{s}}) = 0. \tag{2.2}$$

$|\boldsymbol{\rho}|^{-1}$ is equal to the local radius of curvature R_c. We are interested in cylinder motion such that the cylinder length, R_c and the arclength over which $\boldsymbol{U}(s, t)$ varies are all large in comparison with the cylinder radius a, and we introduce a small parameter ϵ which is order a/R_c.

The irrotational flow induced by the cylinder motion may be described by a velocity potential $\phi(\boldsymbol{x}, t)$. Since the Mach number of the cylinder motion is low, the

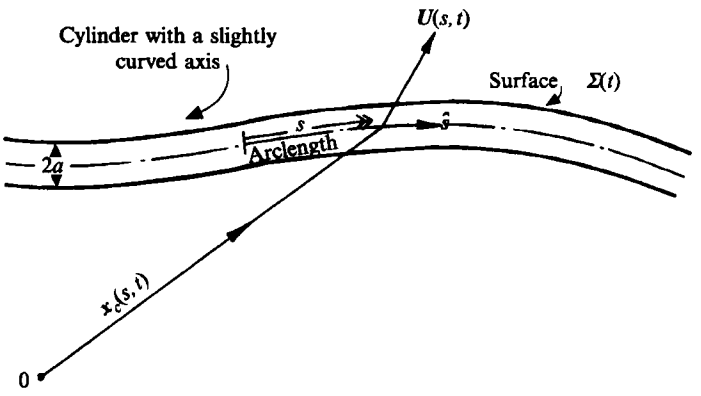

FIGURE 1. The geometry of the cylinder.

flow can be considered to be incompressible and the velocity potential $\phi(\boldsymbol{x}, t)$ at a position $\boldsymbol{x}$ therefore satisfies

$$\nabla^2\phi = 0, \tag{2.3}$$

with boundary conditions

$$\boldsymbol{n}\cdot\nabla\phi = \boldsymbol{n}\cdot\boldsymbol{U} \quad \text{on the cylinder} \tag{2.4}$$

and

$$\phi \to O(|\boldsymbol{x}|^{-2}) \tag{2.5}$$

for $|\boldsymbol{x}|$ large in comparison with the cylinder length. Since the cylinder has no circulation, ϕ is to be single-valued.

The free-space Green function for Laplace's equation can be used to write down a global solution for $\phi(\boldsymbol{x}, t)$ in terms of ϕ on $\Sigma(t)$, the surface of the cylinder:

$$\phi(\boldsymbol{x}, t) = -\frac{1}{4\pi}\int_{\Sigma(t)}\left(\frac{\boldsymbol{n}\cdot\boldsymbol{U}}{|\boldsymbol{x}-\boldsymbol{y}|} - \phi\frac{\boldsymbol{n}\cdot(\boldsymbol{x}-\boldsymbol{y})}{|\boldsymbol{x}-\boldsymbol{y}|^3}\right)\mathrm{d}\Sigma(\boldsymbol{y}). \tag{2.6}$$

We will solve this integral equation for ϕ by investigating the form of $\phi(\boldsymbol{x}, t)$ at positions $\boldsymbol{x}$ which are near the cylinder on the scale of the radius of curvature.

For a position $\boldsymbol{x}$ in the near field close to the cylinder, it is convenient to introduce two parameters, $S(\boldsymbol{x}, t)$ and $\boldsymbol{X}(\boldsymbol{x}, t)$, which are illustrated in figure 2. $S(\boldsymbol{x}, t)$ is the arclength position of the base of a perpendicular from the cylinder axis to $\boldsymbol{x}$, i.e. $S(\boldsymbol{x}, t)$ is a solution of

$$(\boldsymbol{x}-\boldsymbol{x}_c(S, t))\cdot\frac{\partial\boldsymbol{x}_c}{\partial s}(S, t) = 0. \tag{2.7}$$

$\boldsymbol{X}(\boldsymbol{x}, t)$, the vector from $\boldsymbol{x}_c(S, t)$ to $\boldsymbol{x}$, is perpendicular to the cylinder axis at $\boldsymbol{x}_c(S, t)$:

$$\boldsymbol{x} = \boldsymbol{X}+\boldsymbol{x}_c(S, t). \tag{2.8}$$

Equation (2.7) has a unique solution for $R = |\boldsymbol{x}| \ll R_c = a\epsilon^{-1}$ and ensures that

$$\boldsymbol{X}\cdot\hat{\boldsymbol{s}}(S, t) = 0 \tag{2.9}$$

as required.

In this near field $R \ll a\epsilon^{-1}$, we seek an expansion of the velocity potential in the form

$$\phi(\boldsymbol{x}, t) = \phi_0(\boldsymbol{x}, t)+\epsilon\phi_1(\boldsymbol{x}, t)+O(\epsilon^2), \tag{2.10}$$

where ϕ_0 and ϕ_1 are of order unity. This expansion is to satisfy Laplace's equation and the boundary condition on the surface of the cylinder in (2.4). Since this is a near-field

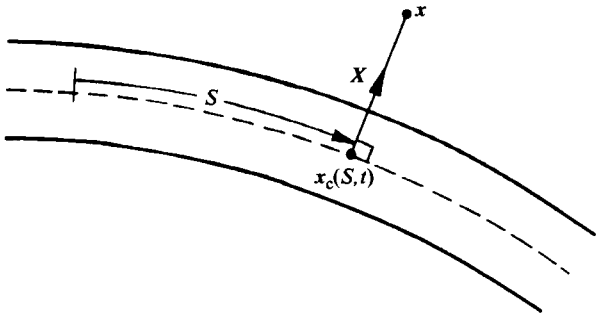

FIGURE 2. The definition of S and X: here $x_c(S,t)$ is the base of a perpendicular, X, from the cylinder axis to x.

solution, we cannot apply the distant boundary condition (2.5). Instead we note that it must match the global solution in (2.6) for $a \ll R \ll a\epsilon^{-1}$.

To lowest order in ϵ, the near-field velocity potential at x is that for a straight cylinder with its axis in the direction $\hat{s}(S,t)$:

$$\phi_0(x,t) = -a^2\frac{\boldsymbol{U}(S,t)\cdot\boldsymbol{X}}{R^2} + A_0 + \sum_{n=1}^{\infty}(A_n\cos n\theta + B_n\sin n\theta)\left(\frac{R^n}{a^n}+\frac{a^n}{R^n}\right). \quad (2.11)$$

$R = |\boldsymbol{X}|$ and θ is an azithumal angle measured around the cylinder axis. The first term on the right-hand side of (2.11) is a solution of Laplace's equation that satisfies the boundary condition (2.4). The remaining terms are the general solution of Laplace's equation with zero normal derivative on $R = a$. The coefficients A_n, B_n are to be determined by matching the form for $\phi_0(x,t)$ in (2.11) to the general representation in (2.6).

A position y on the surface of the cylinder can be expressed in the form $y = x_c(S_y,t) + na$. Hence, for $R \gg a$, the integrand in (2.6) simplifies and

$$\phi(x,t) = -\frac{1}{4\pi}\int\left(\frac{\boldsymbol{n}\cdot\boldsymbol{U}}{|\boldsymbol{d}|}+\frac{a(\boldsymbol{n}\cdot\boldsymbol{U})(\boldsymbol{n}\cdot\boldsymbol{d})}{|\boldsymbol{d}|^3}-\phi\frac{\boldsymbol{n}\cdot\boldsymbol{d}}{|\boldsymbol{d}|^3}\right)\mathrm{d}\Sigma(y)+O\left(\frac{Ua^3}{R^2}\right), \quad (2.12)$$

where $\boldsymbol{d} = \boldsymbol{x} - \boldsymbol{x}_c(S_y,t)$. To evaluate this integral to zeroth order in ϵ, we substitute for ϕ_0 on the cylinder surface from (2.11). Integration is then straightforward for $a \ll R \ll a\epsilon^{-1}$ and gives

$$\phi_0(x,t) = -a^2\frac{\boldsymbol{U}\cdot\boldsymbol{X}}{R^2} + (A_1\cos\theta + B_1\sin\theta)\frac{a}{R} + O\left(\frac{Ua^3}{R^2}\right). \quad (2.13)$$

This is to match to the near-field form in (2.11). Since the near-field form has a term which grows in R like $(A_n\cos n\theta + B_n\sin n\theta)\,R^n/a^n$ if either A_n or B_n is non-zero, we must have $A_n = B_n = 0$ for all $n \geqslant 1$. Hence,

$$\phi_0(x,t) = -a^2\frac{\boldsymbol{U}\cdot\boldsymbol{X}}{R^2} \quad \text{for} \quad R \ll a\epsilon^{-1}. \quad (2.14)$$

To lowest order in ϵ, the near-field velocity potential is just that due to a straight cylinder with velocity $\boldsymbol{U}(S,t)$ and its axis in the direction $\hat{s}(S,t)$. We now wish to go on to determine an expression for the near-field velocity potential which is correct to order ϵ.

Substitution of (2.10) into Laplace's equation (2.3) and the boundary condition (2.4) leads to

$$\epsilon\nabla^2\phi_1 = -\nabla^2\phi_0 + O(\epsilon^2), \tag{2.15}$$

together with

$$\epsilon\boldsymbol{n}\cdot\nabla\phi_1 = \boldsymbol{n}\cdot\boldsymbol{U} - \boldsymbol{n}\cdot\nabla\phi_0 + O(\epsilon^2) \quad \text{on the cylinder.} \tag{2.16}$$

The derivatives of ϕ_0 need to be evaluated correct to order ϵ before we can proceed any further. Differentiation of (2.7) with respect to x_j shows that

$$\frac{\partial S}{\partial x_j} = \frac{\hat{s}_j}{1-\boldsymbol{X}\cdot\boldsymbol{\rho}}. \tag{2.17}$$

It then follows from (2.8) that

$$\frac{\partial X_i}{\partial x_j} = \delta_{ij} - \frac{\hat{s}_i\hat{s}_j}{1-\boldsymbol{X}\cdot\boldsymbol{\rho}}. \tag{2.18}$$

Differentiation of (2.14) gives

$$\frac{\partial\phi_0}{\partial x_i} = -a^2U_j\frac{\partial X_k}{\partial x_i}\frac{\partial}{\partial X_k}\left(\frac{X_j}{R^2}\right) - a^2\frac{\partial U_j}{\partial s}\frac{\partial S}{\partial x_i}\frac{X_j}{R^2}. \tag{2.19}$$

After substituting for the derivatives of S and $\boldsymbol{X}$ from (2.17) and (2.18) respectively and expanding the derivative $\partial(X_j/R^2)/\partial X_k$, this becomes

$$\frac{\partial\phi_0}{\partial x_i} = -a^2\left(\frac{U_i}{R^2} - \frac{2(\boldsymbol{U}\cdot\boldsymbol{X})X_i}{R^4}\right) + \frac{a^2}{1-\boldsymbol{X}\cdot\boldsymbol{\rho}}\frac{(\boldsymbol{U}\cdot\hat{\boldsymbol{s}})\hat{s}_i}{R^2} - a^2\frac{\partial U_j}{\partial s}\frac{X_j\hat{s}_i}{R^2} + O(\epsilon^2), \tag{2.20}$$

after the orthogonality condition (2.9) has been used.

Hence on the surface of the cylinder, where $R = a$ and $\boldsymbol{n} = \boldsymbol{X}/a$, $\boldsymbol{n}\cdot\nabla\phi_0 = \boldsymbol{n}\cdot\boldsymbol{U}$ and the boundary condition (2.16) for ϕ_1 simplifies to

$$\epsilon\boldsymbol{n}\cdot\nabla\phi_1 = O(\epsilon^2). \tag{2.21}$$

Differentiating (2.20) with respect to x_i, and use of the inextensibility condition (2.1) and the orthogonality conditions (2.2) and (2.9), lead to

$$\nabla^2\phi_0 = -\frac{2a^2}{R^4}(\boldsymbol{U}\cdot\boldsymbol{X})(\boldsymbol{\rho}\cdot\boldsymbol{X}) + \frac{a^2}{R^2}\boldsymbol{U}\cdot\boldsymbol{\rho} + O(\epsilon^2). \tag{2.22}$$

The problem for ϕ_1 therefore consists of finding the solution to

$$\epsilon\nabla^2\phi_1 = \frac{2a^2}{R^4}(\boldsymbol{U}\cdot\boldsymbol{X})(\boldsymbol{\rho}\cdot\boldsymbol{X}) - \frac{a^2}{R^2}\boldsymbol{U}\cdot\boldsymbol{\rho}, \tag{2.23}$$

correct to order ϵ, which satisfies the boundary condition (2.21).

We note that $-\frac{1}{2}a^2(\boldsymbol{U}\cdot\boldsymbol{X})(\boldsymbol{\rho}\cdot\boldsymbol{X})/R^2$ is a particular integral of (2.23), and that the general solution that satisfies the boundary condition (2.21) can be expressed in the form

$$\epsilon\phi_1(\boldsymbol{x},t) = -\frac{a^2}{R^2}(\boldsymbol{U}\cdot\boldsymbol{X})(\boldsymbol{\rho}\cdot\boldsymbol{X}) + \epsilon C_0 + \sum_{n=1}^{\infty}\epsilon(C_n\cos n\theta + D_n\sin n\theta)\left(\frac{R^n}{a^n} + \frac{a^n}{R^n}\right). \tag{2.24}$$

The coefficients C_n and D_n are to be determined by matching to the large-R/a form of the general representation in (2.12).

After substituting for ϕ_0 and ϕ_1 from (2.14) and (2.24) into the integrand in (2.12), the surface integrals can be evaluated correct to $O(\epsilon)$ for $a \ll R \ll a\epsilon^{-1}$, to give

$$\phi_0(\boldsymbol{x},t)+\epsilon\phi_1(\boldsymbol{x},t) = -\frac{a^2}{R^2}\boldsymbol{U}\cdot\boldsymbol{X}-\frac{a^2}{2R^2}(\boldsymbol{U}\cdot\boldsymbol{X})(\boldsymbol{\rho}\cdot\boldsymbol{X})+\frac{a^2}{2}\boldsymbol{U}\cdot\boldsymbol{\rho} + \epsilon(C_1\cos\theta+D_1\sin\theta)\frac{a}{R}+O\left(\frac{Ua^3}{R^2}\right). \quad (2.25)$$

Since this is to match the near-field forms in (2.14) and (2.24), we must have $\epsilon C_0 = \frac{1}{2}a^2\,\boldsymbol{U}\cdot\boldsymbol{\rho}$ and $C_n = D_n = 0$ for $n \geqslant 1$.

Collecting together ϕ_0 and ϕ_1, from (2.14) and (2.24) respectively, gives the velocity potential correct to order ϵ:

$$\phi(\boldsymbol{x},t) = -\frac{a^2}{R^2}\boldsymbol{U}\cdot\boldsymbol{X}-\frac{a^2}{2R^2}(\boldsymbol{U}\cdot\boldsymbol{X})(\boldsymbol{\rho}\cdot\boldsymbol{X})+\frac{a^2}{2}\boldsymbol{U}\cdot\boldsymbol{\rho}+O(\epsilon^2). \quad (2.26)$$

The local fluid velocity, $\boldsymbol{u}(\boldsymbol{x},t)$, follows from (2.20) and the derivative of (2.26):

$$\boldsymbol{u}(\boldsymbol{x},t) = -a^2\left(\frac{\boldsymbol{U}-(\boldsymbol{U}\cdot\hat{\boldsymbol{s}})\hat{\boldsymbol{s}}}{R^2}-\frac{2(\boldsymbol{U}\cdot\boldsymbol{X})\boldsymbol{X}}{R^4}\right)-a^2\frac{\partial U_j}{\partial s}\frac{X_j\hat{\boldsymbol{s}}}{R^2}-\frac{a^2(\boldsymbol{U}\cdot\boldsymbol{X})\boldsymbol{\rho}}{2R^2} + \boldsymbol{X}\cdot\boldsymbol{\rho}a^2\left(\frac{3(\boldsymbol{U}\cdot\hat{\boldsymbol{s}})\hat{\boldsymbol{s}}}{2R^2}-\frac{\boldsymbol{U}}{2R^2}+\frac{(\boldsymbol{U}\cdot\boldsymbol{X})\boldsymbol{X}}{R^4}\right). \quad (2.27)$$

The velocity field in (2.27) describes the irrotational flow due to the motion of a cylinder with a slightly curved axis. This result is used in §4. The complete velocity field can be decomposed into the sum of an irrotational component, which has been determined in this section, and a term induced by vorticity, which is investigated in §3.

3. The pressure field generated by vorticity near the cylinder

The two-dimensional velocity potential due to a line vortex parallel to a cylinder axis is well known (see for example Batchelor 1967, p. 423). We seek to generalize that result to determine the three-dimensional velocity potential generated by an arbitrary distribution of vorticity near a moving cylinder. This will subsequently be used to calculate the induced pressure field.

At positions $\boldsymbol{x}$ close to both the vorticity and the cylinder, the cylinder may be considered as straight and moving with a uniform velocity, $\boldsymbol{U}(t)$ say, if we neglect terms of order ϵ. It is convenient to view this flow from an accelerating reference frame in which the cylinder is locally at rest and there is a flow $-\boldsymbol{U}$ from infinity. Let

$$\boldsymbol{x}' = \boldsymbol{x}-\int_0^t \boldsymbol{U}(\tau)\,\mathrm{d}\tau, \quad \boldsymbol{v}' = \boldsymbol{v}-\boldsymbol{U}. \quad (3.1)$$

Outside the regions of vorticity we can introduce a potential $\phi'(\boldsymbol{x}',t)$ for $\boldsymbol{v}'$, the fluid velocity in the moving reference frame, and write

$$\boldsymbol{v}' = \nabla\phi'. \quad (3.2)$$

We seek to find an expression for $\phi'(\boldsymbol{x}',t)$ in terms of the cylinder velocity $\boldsymbol{U}(t)$ and the vorticity $\boldsymbol{\omega}$. The flows of interest are of high Reynolds number and the convection of vorticity is more significant than its diffusion. It is therefore appropriate to use an

inviscid form of the momentum equation. We find $B(x', t)$ to be a convenient dependent variable:

$$B(x', t) = (p - p_\infty)/\rho + \tfrac{1}{2}v'^2 - \tfrac{1}{2}U^2 + \dot{U}\cdot x', \tag{3.3}$$

where p is the pressure and ρ the density. The momentum equation can then be written in the form

$$\frac{\partial B}{\partial x_i'} = -(\omega \times v')_i - \left.\frac{\partial v_i'}{\partial t}\right|_{x'}. \tag{3.4}$$

The variable $B(x', t)$ is convenient because, although it is defined everywhere, outside the regions of vorticity

$$B = -\left.\frac{\partial \phi'}{\partial t}\right|_{x'}, \tag{3.5}$$

a result which can be readily seen from a comparison of (3.2) and (3.4). We seek a representation theorem for $B(x', t)$ in terms of the cylinder velocity and the vorticity. The velocity potential will then follow after integration with respect to time.

First, note that a vorticity equation can be derived by taking the curl of (3.4) to give

$$\left.\frac{\partial \omega}{\partial t}\right|_{x'} = -\operatorname{curl}(\omega \times v'). \tag{3.6}$$

It is shown in Appendix A how the velocity field v' can be expressed entirely in terms of the cylinder velocity and the vorticity. This is analogous to the work of Lighthill (1956) for vorticity near a rigid sphere. For a specific cylinder velocity, (3.6) can be integrated with respect to time to determine the development of an initial distribution of vorticity. We therefore consider the vorticity field to be prescribed.

It follows from the divergence of (3.4) and the continuity equation that

$$\nabla^2 B = -\operatorname{div}(\omega \times v'). \tag{3.7}$$

This is to be solved subject to the boundary condition that the surface of the cylinder is impenetrable, so that

$$n\cdot v' = 0 \quad \text{on} \quad \Sigma. \tag{3.8}$$

The cylinder is at rest in the x'-frame and, after differentiation of (3.8) with respect to time, (3.4) shows that

$$n\cdot\nabla B = -n\cdot(\omega \times v') \quad \text{on} \quad \Sigma. \tag{3.9}$$

It is evident from the definition of B in (3.3) that far from the cylinder

$$B \to \dot{U}\cdot x' \quad \text{as} \quad x' \to \infty. \tag{3.10}$$

Equation (3.7) together with the boundary conditions (3.9) and (3.10) completely define $B(x', t)$. We will solve these equations to find $B(x', t)$ (and hence $\phi'(x', t)$) in terms of the vorticity, $\omega(x', t)$. It is convenient to decompose $B(x', t)$ into two parts by writing

$$B(x', t) = B_u(x', t) + B_\omega(x', t), \tag{3.11}$$

where $\nabla^2 B_u = 0$, with $n\cdot\nabla B_u = 0$ on Σ, $B_u \to \dot{U}\cdot x'$ as $x' \to \infty$ (3.12)

and

$$\nabla^2 B_\omega = -\operatorname{div}(\omega \times v'), \quad \text{with} \quad n\cdot\nabla B_\omega = -n\cdot(\omega \times v') \quad \text{on} \quad \Sigma, \quad B_\omega \to 0 \quad \text{as} \quad x' \to \infty. \tag{3.13}$$

$B_u(x', t)$ is the contribution to $B(x', t)$ from the cylinder motion and its solution can be written down immediately:

$$B_u(x', t) = \dot{U}\cdot x' + \dot{U}_R a^2/R, \tag{3.14}$$

where (x_1', R, θ) are cylindrical polar coordinates of the position vector x', the 1-direction being taken parallel to the local cylinder axis. The suffix R denotes the radial component, i.e. $U_R = U_2 \cos\theta + U_3 \sin\theta$. The velocity potential ϕ_u' can be found from an integration of (3.5) and is given by

$$\phi_u'(x', t) = -U\cdot x' - U_R a^2/R. \tag{3.15}$$

$B_\omega(x', t)$ is the contribution to $B(x', t)$ from the vorticity field. It can be determined most conveniently by introducing a Green function $G(y' \mid x')$ which satisfies

$$\nabla_{y'}^2 G = \delta(y' - x'), \quad \text{with} \quad n\cdot\nabla G = 0 \quad \text{on} \quad \Sigma, \quad G \to 0 \quad \text{as} \quad y' \to \infty. \tag{3.16}$$

After a standard application of Green's theorem, (3.13) and (3.16) lead to

$$B_\omega(x', t) = \int (\omega \times v')\cdot\nabla_{y'} G \, \mathrm{d}^3 y'. \tag{3.17}$$

We now make use of the technique introduced by Möhring (1978) to rewrite this equation in a way that expresses $B_\omega(x', t)$ in terms of vorticity alone.

We restrict (x', t) to positions for which the vorticity is zero. Then $B(x', t) = -\partial\phi'/\partial t\,|_{x'}$ as shown in (3.5). Moreover $\nabla_{y'}^2 G = 0$ at all non-zero values of the integrand in (3.17) and so a vector Green function $G(y' \mid x')$ can be introduced, defined by

$$\text{curl } G = \text{grad } G \quad \text{for} \quad y' \neq x'. \tag{3.18}$$

G is calculated in Appendix B.

Rewriting (3.17) in terms of this vector Green function gives

$$-\left.\frac{\partial \phi_\omega'}{\partial t}\right|_{x'} = \int (\omega \times v')\cdot \text{curl } G \, \mathrm{d}^3 y', \tag{3.19}$$

which after integration by parts becomes

$$\left.\frac{\partial \phi_\omega'}{\partial t}\right|_{x'} = -\int \text{curl } (\omega \times v')\cdot G \, \mathrm{d}^3 y'. \tag{3.20}$$

The vorticity equation (3.6) shows that this reduces to

$$\left.\frac{\partial \phi_\omega'}{\partial t}\right|_{x'} = \frac{\partial}{\partial t}\int \omega\cdot G \, \mathrm{d}^3 y'. \tag{3.21}$$

After integration with respect to time, we finally obtain

$$\phi_\omega'(x', t) = \int \omega\cdot G \, \mathrm{d}^3 y'. \tag{3.22}$$

Changes in $\int \omega\cdot G \, \mathrm{d}^3 y'$ generate fluctuations in the velocity potential. Now the vector Green function $G(y' \mid x')$ is independent of time, while the vorticity satisfies a

conservation relationship that $\int \boldsymbol{\omega}\cdot\mathbf{d}S$ is constant for any material surface S. Equation (3.22) therefore shows that both vortex stretching and the convection of vorticity across contours of constant G produce fluctuations in velocity potential.

Substitution for G in (3.22) from Appendix B equation (B 6) leads to

$$\phi'_\omega(\boldsymbol{x}',t) = \frac{\mathrm{i}a}{(2\pi)^2}\int \sum_{n=-\infty}^{\infty}\left(\frac{\omega_\psi P_n}{k\sigma}-\omega_1 nQ_n\right)\kappa(I_n(\kappa R)\,\dot{K}_n(\kappa a)-\dot{I}_n(\kappa a)\,K_n(\kappa R)) \times \mathrm{e}^{\mathrm{i}k(y'_1-x'_1)+\mathrm{i}n(\psi-\phi)}\,\mathrm{d}k\,\mathrm{d}^3\boldsymbol{y}', \quad (3.23)$$

for $R<\sigma$. In (3.23) $\kappa=|k|$ and $I_n(z)$ and $K_n(z)$ are modified Bessel functions. A dot denotes differentiation with respect to the argument. (y'_1,σ,ψ) and $(\omega_1,\omega_\sigma,\omega_\psi)$ are the cylindrical polar coordinates of $\boldsymbol{y}'$ and $\boldsymbol{\omega}$ respectively and

$$P_n = \frac{1}{\kappa a\dot{K}_n(\kappa a)}\int_{\kappa\sigma}^{\infty} zK_n(z)\,\mathrm{d}z \quad\text{and}\quad Q_n = \frac{1}{\kappa a\dot{K}_n(\kappa a)}\int_{\kappa\sigma}^{\infty}\frac{K_n(z)}{z}\,\mathrm{d}z. \quad (3.24)$$

The total velocity potential is given by the addition of (3.15) and (3.23):

$$\begin{aligned}\phi'(\boldsymbol{x}',t) &= \phi'_u(\boldsymbol{x}',t)+\phi'_\omega(\boldsymbol{x}',t)\\ &= -\boldsymbol{U}\cdot\boldsymbol{x}'-U_R\frac{a^2}{R}+\frac{\mathrm{i}a}{(2\pi)^2}\int\sum\left(\frac{\omega_\psi P_n}{k\sigma}-\omega_1 nQ_n\right)\kappa(I_n(\kappa R)\,\dot{K}_n(\kappa a)-\dot{I}_n(\kappa a)\,K_n(\kappa R))\\ &\qquad\times \mathrm{e}^{\mathrm{i}k(y'_1-x'_1)+\mathrm{i}n(\psi-\theta)}\,\mathrm{d}k\,\mathrm{d}^3\boldsymbol{y}' \quad\text{for}\quad R<\sigma. \quad (3.25)\end{aligned}$$

This is a main result of this paper. It extends the well-known formula for the velocity potential due to a line vortex parallel to a cylinder axis to an arbitrary, unsteady three-dimensional distribution of vorticity near a moving cylinder. This velocity potential gives a convenient description of the flow field, which we will use to determine the pressure.

Equation (3.3) shows how the pressure field can be expressed entirely in terms of $\boldsymbol{v}'$ and B. We note from (3.2) and (3.5) that these can be readily calculated by differentiation of (3.25) with respect to $\boldsymbol{x}'$ and $-t$ respectively. We are particularly interested in the pressure perturbation on the surface of the cylinder and substitution for $\boldsymbol{v}'$ and B into (3.3) yields

$$\begin{aligned}\frac{(p-p_\infty)(x_1,a,\theta)}{\rho} &= a\dot{U}_R+\tfrac{1}{2}U_R^2-\tfrac{3}{2}U_\theta^2+\frac{\mathrm{i}}{(2\pi)^2}\int\sum\left(\frac{\dot{\omega}_\psi P_n}{k\sigma}-\dot{\omega}_1 nQ_n\right)\mathrm{e}^{\mathrm{i}k(y'_1-x'_1)+\mathrm{i}n(\psi-\theta)}\,\mathrm{d}k\,\mathrm{d}^3\boldsymbol{y}'\\ &\quad-\frac{1}{(2\pi)^2 a}\int\sum\left(\frac{\omega_\psi P_n}{k\sigma}-\omega_1 nQ_n\right)(U_1 ka+2U_\theta n)\,\mathrm{e}^{\mathrm{i}k(y'_1-x'_1)+\mathrm{i}n(\psi-\theta)}\,\mathrm{d}k\,\mathrm{d}^3\boldsymbol{y}'. \quad (3.26)\end{aligned}$$

U_θ is the azimuthal velocity, $U_\theta=-U_2\sin\theta+U_3\cos\theta$. Vorticity at the cylinder surface has been neglected in deriving this expression. We are considering a cylinder whose motion, over a prolonged period, had led to significant vorticity away from the surface. Equation (3.26) describes the surface pressures induced by this vorticity. The vorticity has been assumed to be weak so that the square of vorticity terms can be neglected in the calculation of pressure.

Embedded transducers within a towed array are used to measure an incoming sound field. They also respond to the flow noise due to vorticity near the cylinder and the characteristics of this noise can be determined from (3.26). The embedded transducers actually measure the circumferentially averaged surface pressure. This information is then used to evaluate the axial-wavenumber decomposition of the measured pressure. We are therefore particularly interested in

$$p_m(-k,t) = \frac{1}{2\pi}\int (p-p_\infty)(x_1', a, \theta)\, \mathrm{e}^{\mathrm{i}kx_1'}\, \mathrm{d}\theta\, \mathrm{d}x_1' \quad \text{for} \quad |k|\, R_c \gg 1. \tag{3.27}$$

Integration of (3.26) leads to

$$p_m(-k,t) = \frac{\mathrm{i}\rho}{2\pi}\int \frac{P_0}{k\sigma}(\dot{\omega}_\psi + \mathrm{i}kU_1\omega_\psi)\, \mathrm{e}^{\mathrm{i}ky_1'}\, \mathrm{d}^3\boldsymbol{y}' + \frac{\rho}{\pi a}\int\left(\omega_1 U_\psi Q_1 - \frac{\mathrm{i}\omega_\psi U_\sigma P_1}{k\sigma}\right)\mathrm{e}^{\mathrm{i}ky_1'}\, \mathrm{d}^3\boldsymbol{y}' \tag{3.28}$$

for $|k|\, R_c \gg 1$.

The vorticity equation (3.6) can be used to replace $\dot{\omega}_\psi$ by $\partial(\boldsymbol{\omega}\times\boldsymbol{v}')_1/\partial\sigma - \partial(\boldsymbol{\omega}\times\boldsymbol{v}')_\sigma/\partial y_1'$ and after integration by parts we obtain

$$p_m(-k,t) = \frac{\rho}{2\pi}\int\left\{\omega_1\left(\frac{v_\psi' P_0}{\sigma} + \frac{2U_\psi Q_1}{a}\right) - \frac{\mathrm{i}\omega_\sigma v_\psi'}{k\sigma}\frac{\partial P_0}{\partial\sigma} + \omega_\psi\left(-\frac{P_0}{\sigma}(v_1' + U_1) + \frac{\mathrm{i}v_\sigma'}{k\sigma}\frac{\partial P_0}{\partial\sigma} - \frac{2\mathrm{i}U_\sigma P_1}{ka\sigma}\right)\right\}\mathrm{e}^{\mathrm{i}ky_1'}\, \mathrm{d}^3\boldsymbol{y}'. \tag{3.29}$$

The measured wavenumber decomposition of the surface pressure is predicted to depend only on the instantaneous velocity and vorticity fields. We determined in Appendix A equation (A 12) how the velocity can be expressed in terms of the instantaneous vorticity and cylinder velocity. Equation (3.29) therefore provides a means of calculating the surface pressure for a particular distribution of vorticity.

The wavenumbers of interest are small in comparison with a^{-1}. Provided the vorticity is concentrated near the cylinder at positions such that $|k|\,\sigma \ll 1$, equation (3.29) simplifies. For small positive $k\sigma$ the functions K_n in the definitions of P_0, P_1 and Q_1 in (3.24) may be expanded by their small-argument asymptotic forms to give

$$p_m(-k,t) = \frac{\rho}{2\pi}\int\{-\omega_1(v_\psi' + (2-\pi k\sigma)U_\psi) + \omega_\sigma\, \mathrm{i}k\sigma\,(\ln(\tfrac{1}{2}k\sigma) + \gamma)v_\psi' + \omega_\psi(v_1' + U_1 - \mathrm{i}k\sigma\,(\ln(\tfrac{1}{2}k\sigma)+\gamma)v_\sigma' + \mathrm{i}(\pi - 2k\sigma)U_\sigma)\}\frac{\mathrm{e}^{\mathrm{i}ky'}}{\sigma}\,\mathrm{d}^3\boldsymbol{y}', \tag{3.30}$$

where γ is Euler's constant and $kR_c \gg 1 \gg ka$.

Equation (3.30) describes the wavenumber decomposition of the circumferentially averaged pressure in terms of the vorticity and velocity fields. Chase & Noiseux (1982) and Dhanak (1988) derived an expression for the pressure in terms of Lighthill's quadrupoles, T_{ij}. However, an explicit dependence on vorticity as in (3.30) is often more convenient because the vortical regions of the flow are much more concentrated than the hydrodynamic region over which T_{ij} is non-zero. Moreover the development of the vorticity field can be described by simple kinematics. The velocity field is then given by equation (A 12).

If we assume that the vorticity is so weak that products of it may be neglected, the

fluid velocity v' in (3.30) may be replaced by $\nabla\phi'_u$, the velocity due to the cylinder motion alone. After using (3.15) we obtain

$$p_m(-k,t) = \frac{\rho}{2\pi}\int\left\{-\omega_1\left(1-\frac{a^2}{\sigma^2}-\pi k\sigma\right)U_\psi - \omega_\sigma\, \mathrm{i}k\sigma\left(1+\frac{a^2}{\sigma^2}\right)(\ln(\tfrac{1}{2}k\sigma)+\gamma)\,U_\psi \right.$$
$$\left. +\omega_\psi\left(\mathrm{i}k\sigma\left(1-\frac{a^2}{\sigma^2}\right)(\ln(\tfrac{1}{2}k\sigma)+\gamma)+\mathrm{i}(\pi-2k\sigma)\right)U_\sigma\right\}\frac{\mathrm{e}^{\mathrm{i}ky'_1}}{\sigma}\,\mathrm{d}^3y'. \quad (3.31)$$

The condition div $\boldsymbol{\omega} = 0$ means that the three vorticity components are interdependent. This can be exploited to simplify the expressions for $p_m(-k,t)$. The details are given in Appendix C, where it is shown that (3.31) is equivalent to

$$p_m(-k,t) = -\frac{\rho}{2\pi}\int(\omega_1 U_\psi + \mathrm{i}k\sigma\omega_\psi U_\sigma)\left(\frac{1}{\sigma}-\frac{a^2}{\sigma^3}\right)\mathrm{e}^{\mathrm{i}ky'_1}\,\mathrm{d}^3y', \quad (3.32)$$

for $|k|R_c \gg 1 \gg |k|a$, where

$$U_\sigma = U_2\cos\psi + U_3\sin\psi \quad \text{and} \quad U_\psi = -U_2\sin\psi + U_3\cos\psi. \quad (3.33)$$

Equation (3.32) is in a particularly convenient form. It gives the wavenumber decomposition of the circumferentially averaged surface pressure directly in terms of the axial and azimuthal components of the instantaneous vorticity.

Note that the integrand in (3.32) tends to zero as the vorticity approaches the cylinder, i.e. as $\sigma \to a$. Any contribution to the surface pressure from surface vorticity was neglected in the derivation of (3.26) and the following equations. We now see that, as vorticity approaches the cylinder, its contribution to the surface pressure becomes unimportant. Essentially this is because the image of the axial or azimuthal vorticity cancels its effect.

Chase & Noiseux (1982) and Dhanak (1988) predicted that the circumferentially averaged surface pressure spectrum should be independent of wavenumber at low wavenumbers. We see from (3.32) that such a term depends on the axial components of vorticity. The more substantial azimuthal vorticity generates a contribution of order $|k|^2a^2$ in the surface pressure spectrum.

Equation (3.32) gives more information than simple scaling laws. It can be used to predict the development of flow noise during a cylinder manoeuvre. We illustrate its use in §4 by investigating two model problems.

4. A vortex ring near a cylinder

In §3 an expression was derived for the surface pressures generated by an arbitrary distribution of vorticity, near a moving cylinder. In this section we demonstrate an application of that theory.

A straight cylinder in axial motion has an established, substantial boundary layer. We are interested in the pressures generated as transverse motion of the cylinder causes the vorticity in this boundary layer to be shed. In seeking a qualitative description of this flow, we take a highly simplified model of an element of vorticity in the boundary layer. We model it by a vortex ring of strength γ_0, which initially lies in the plane $x_1 = 0$, is circular with radius b and coaxial with the cylinder. The initial vorticity can be expressed in the form $\boldsymbol{\omega}(\boldsymbol{x},0) = \gamma_0\,\delta(R-b)\,\delta(x_1)\,\boldsymbol{e}_{\psi_0}$, where x_1, R, and ψ_0 are cylindrical polar coordinates centred on the initial position of the vortex. $\boldsymbol{e}_{\psi_0}$ is the azimuthal unit tangent vector. At times $t > 0$, the vorticity is convected in a velocity field $\boldsymbol{v}(\boldsymbol{x},t)$ and the ring deforms.

The initial polar angle ψ_0 is a convenient Lagrangian variable. Let us suppose that at time t the element of the ring which was initially at ψ_0 has moved to $\boldsymbol{x}_v(\psi_0, t)$. Since, in an inviscid fluid, vorticity convects with the fluid particles

$$\left.\frac{\partial \boldsymbol{x}_v}{\partial t}\right|_{\psi_0} = \boldsymbol{v}(\boldsymbol{x}_v(\psi_0, t), t). \tag{4.1}$$

The vorticity is parallel to the ring, that is parallel to the tangential direction $\partial \boldsymbol{x}_v/\partial \psi_0$. $|\partial \boldsymbol{x}_v/\partial \psi_0|$ describes the length of a material line coinciding with the vortex line. Since the ratio between the local vorticity magnitude and the length of such a material line remains constant (Batchelor 1967, p. 275), we can write

$$\boldsymbol{\omega}(\boldsymbol{x}, t) = \gamma_0 \int_0^{2\pi} \frac{\partial \boldsymbol{x}_v}{\partial \psi_0} \delta(\boldsymbol{x} - \boldsymbol{x}_v(\psi_0, t))\, \mathrm{d}\psi_0, \tag{4.2}$$

where $\boldsymbol{x}_v(\psi_0, t)$ is to be determined from integration of (4.1), with the initial condition $x_{v1} = 0$, $R = b$ and $\psi = \psi_0$.

We will assume that the vorticity is so weak that any products of γ_0 may be neglected. The neglect of any self-induction means that, although small, the vortex core size ϵ is non-zero, and the vortex strength γ_0 is sufficiently weak to ensure that $(\gamma_0/b) \ln (b/\epsilon)$ is small in comparison with the fluid velocity induced by the cylinder motion (Batchelor 1967, p. 523). Then the convection velocity $\boldsymbol{v}$ in (4.1) may be replaced by $\boldsymbol{u}$, the fluid velocity due to potential flow around the cylinder, given in (2.27).

The axial wavenumber decomposition of the circumferentially averaged surface pressure can be obtained by substituting for the vorticity in (3.32). Equation (3.32) shows that, as far as its influence on $p_m(-k, t)$ is concerned, vorticity distributed over a small but finite core may be treated as concentrated provided $\mathrm{e}^{\mathrm{i}k_1 y_1}$, ψ and $1 - a^2/\sigma^2$ do not vary appreciably over the core. For the vorticity distribution in (4.2)

$$p_m(-k, t) = -\frac{\rho \gamma_0}{2\pi} \int_0^{2\pi} \left(\frac{\partial x_{v1}}{\partial \psi_0} U_{\psi_v} + \mathrm{i}k\sigma_v^2 \frac{\partial \psi_v}{\partial \psi_0} U_{\sigma_v} \right) \left(\frac{1}{\sigma_v} - \frac{a^2}{\sigma_v^3} \right) \mathrm{e}^{\mathrm{i}k x'_{v1}}\, \mathrm{d}\psi_0, \tag{4.3}$$

where $(x'_{v1}, \sigma_v, \psi_v)$ are the local cylindrical polar coordinates of

$$\boldsymbol{x}'_v = \boldsymbol{x}_v(\psi_0, t) - \int_0^t \boldsymbol{U}(\tau)\, \mathrm{d}\tau.$$

The first term on the right-hand side of (4.3) depends on axial vorticity and would also arise in the two-dimensional case of an axial line vortex near a straight cylinder. That two-dimensional problem can be solved in a straightforward way using complex variable theory, and provides a reassuring check on the algebra.

We will consider two particular examples in some detail. The first investigates the effects of transverse motion of a straight cylinder on a vortex ring, while the second highlights the first-order effects of curvature of the cylinder axis.

4.1. *A straight cylinder*

Consider a cylinder of radius a with a uniform, but unsteady velocity $\boldsymbol{U}(t)$ whose axis is in the 1-direction. Then

$$\hat{\boldsymbol{s}} = (1, 0, 0), \quad \boldsymbol{p} \equiv 0 \quad \text{and} \quad \boldsymbol{x}_c(s, t) = (s, 0, 0) + \int_0^t \boldsymbol{U}(\tau)\, \mathrm{d}\tau.$$

The fluid velocity induced by cylinder motion, described by (2.27), simplifies considerably and when substituted into (4.1) leads to

$$\left.\frac{\partial x'_{v1}}{\partial t}\right|_{\psi_0} = -U_1(t), \tag{4.4a}$$

$$\left.\frac{\partial \sigma_v}{\partial t}\right|_{\psi_0} = U_T \cos(\psi_v - \alpha)\left(\frac{a^2}{\sigma_v^2} - 1\right) \tag{4.4b}$$

and

$$\left.\frac{\partial \psi_v}{\partial t}\right|_{\psi_0} = U_T \sin(\psi_v - \alpha)\left(\frac{a^2}{\sigma_v^2} + 1\right)\frac{1}{\sigma_v}. \tag{4.4c}$$

$U_T(t)$, the transverse speed of the cylinder, is at an angle α to the plane $\psi_v = 0$.

Integration of (4.4), from the initial conditions

$$x_{v1}(\psi_0, 0) = 0, \quad \sigma_v(\psi_0, 0) = b \quad \text{and} \quad \psi_v(\psi_0, 0) = \psi_0, \tag{4.5}$$

determines the subsequent shape of the vortex.

If the transverse cylinder motion is rectilinear we can, without loss of generality, take $\alpha = 0$. The right-hand sides of (4.4*b*) and (4.4*c*) clearly depend on the functional form of the cylinder velocity. However, this explicit dependence can be eliminated by introducing a new time-like variable T defined by

$$T = \int_0^t U_T(\tau)\, \mathrm{d}\tau / a.$$

T is the instantaneous transverse displacement of the cylinder, non-dimensionalized with respect to the cylinder radius. Rewriting (4.4*b*, *c*) in terms of T for $\alpha = 0$, we obtain

$$\left.\frac{1}{a}\frac{\partial \sigma_v}{\partial T}\right|_{\psi_0} = \cos\psi_v\left(\frac{a^2}{\sigma_v^2} - 1\right), \quad \left.\frac{\partial \psi_v}{\partial T}\right|_{\psi_0} = \sin\psi_v\left(\frac{a^2}{\sigma_v^2} + 1\right)\frac{a}{\sigma_v}. \tag{4.6a, b}$$

These two equations can be integrated numerically using a Runge–Kutta–Merson method, thus determining the shape of the vortex ring for an arbitrary velocity $U_T(t)$. Some results are shown in figure 3.

Since there is no distortion of the vortex in the 1-direction, the constraints that the vortex moves with the fluid and that the fluid is incompressible mean that the area between the vortex ring and the cylinder remains constant, i.e.

$$\frac{1}{2}\int_0^{2\pi} (\sigma_v^2 - a^2)\, \mathrm{d}\psi_v = \pi(b^2 - a^2). \tag{4.7}$$

As a check on the accuracy of the numerical integration, the integral in (4.7) was evaluated numerically at each time T and compared with $\pi(b^2 - a^2)$.

It is possible to solve (4.6) analytically when $(\sigma_v - a)/a$ is small. The details are given in Dowling (1993), where it is shown that

$$\sigma_v(\psi_v, T) - a = (b-a)\,\mathrm{e}^{-2T}\frac{1 + \tan^2(\psi_v/2)}{1 + \mathrm{e}^{-4T}\tan^2(\psi_v/2)} + aO(\sigma_v/a - 1)^2. \tag{4.8}$$

This expression shows that, except near $\psi_v = \pi$, $\sigma_v(\psi_v, T)$ rapidly approaches a as T tends to infinity. Near $\psi_v = \pi$, $\tan(\psi_v/2)$ is large and (4.8) predicts that $\sigma_v - a$ grows exponentially. However, these results near $\psi_v = \pi$ have very limited applicability since the assumption that $(\sigma_v - a)/a$ is small is soon violated. This approximate solution is

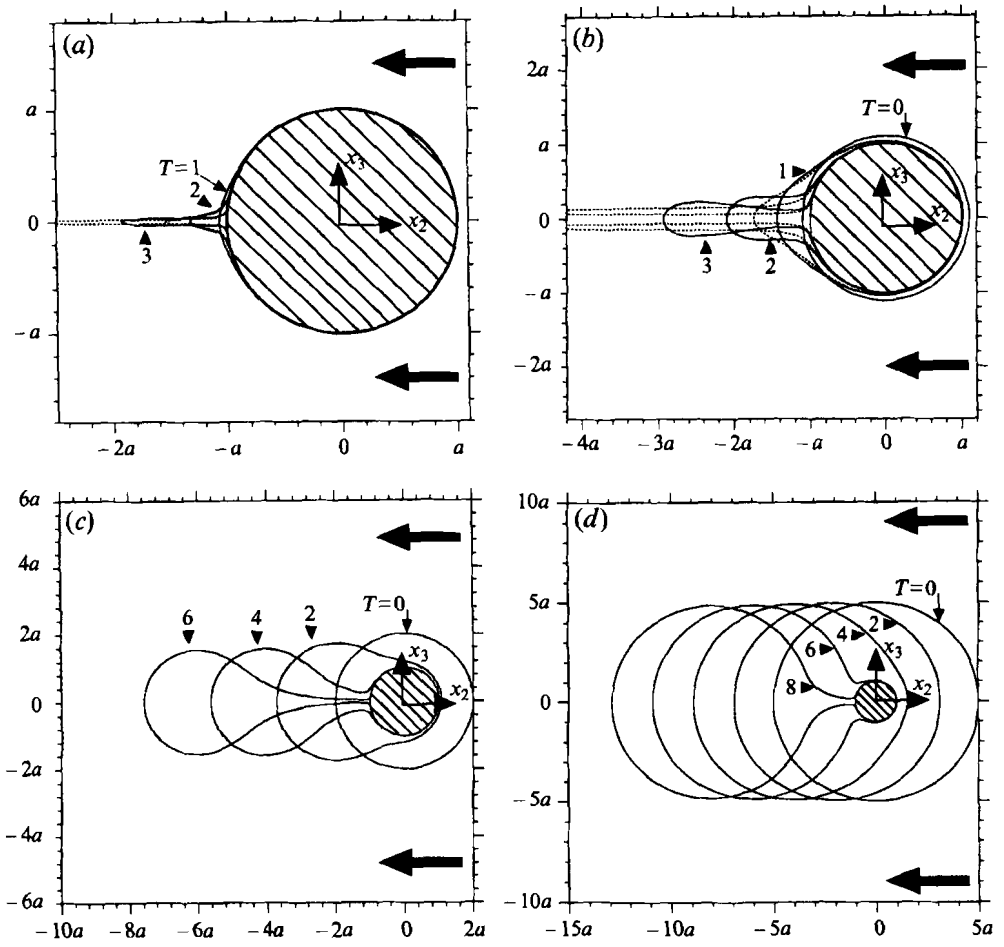

FIGURE 3. The position of the vortex ring in the $x_1 = 0$ plane at various non-dimensional times, T, for (*a*) $b = 1.01a$, (*b*) $b = 1.1a$, (*c*) $b = 2a$, (*d*) $b = 5a$. ——, Numerical integration of (4.6); ....., small-$(\sigma_v - a)/a$ approximation (equation (4.8)).

compared with the numerical results for the shape of the vortex ring in figure 3. We see that for small $(b-a)/a$ it is a good approximation for most ψ_v, except near $\psi_v = \pi$, where it soon over-estimates the distortion.

The vortex ring position can also be determined analytically for the two angles $\psi_v = 0$ and π. For these angles (4.6) shows that $\partial\psi_v/\partial T = 0$ and

$$\frac{1}{a}\frac{\partial\sigma_v}{\partial T} = \pm\left(\frac{a^2}{\sigma_v^2} - 1\right), \tag{4.9}$$

where the upper sign is for $\psi_v = 0$ and the lower sign for $\psi_v = \pi$. Integration of (4.9) gives

$$\sigma_v - b + \frac{a}{2}\ln\left(\frac{(\sigma_v - a)(b+a)}{(\sigma_v + a)(b-a)}\right) = \mp aT. \tag{4.10}$$

The results for the vortex ring shape in figure 3 are in a moving reference frame centred on the cylinder. In this frame of reference there is an incoming flow from the right. It is apparent that the relative motion between the cylinder and the flow essentially causes

the vortex ring to be shed. Of course, impenetrable surfaces like the cylinder cannot cut through vorticity which moves with the fluid and, while most of the vorticity is shed, a small remnant of the vortex ring remains wrapped around the cylinder. Except when $(b-a)/a$ is small, the vortex ring is essentially shed from the cylinder by the non-dimensional time $T = b/a$. This is not really surprising. Since T is the displacement of the cylinder non-dimensionalized with respect to a, at a time $T = b/a$ the cylinder has just reached the initial vortex position. Hence we can conclude that transverse cylinder motion causes boundary-layer vorticity to be shed from a cylinder once the displacement of the axis of the cylinder exceeds the initial boundary-layer thickness. We will now calculate the pressures generated by this shedding process.

Substituting

$$U_{\sigma_v} = U_T(t)\cos\psi_v \quad \text{and} \quad x'_{v1} = -\int_0^t U_1(\tau)\,\mathrm{d}\tau,$$

from (3.33) and (4.4), into (4.3) leads to

$$p_m(-k,t) = \frac{\mathrm{i}ka\rho\gamma_0}{2\pi}\exp\left(-\mathrm{i}k\int_0^t U_1(\tau)\,\mathrm{d}\tau\right)U_T(t)F(T), \tag{4.11}$$

where

$$F(T) = -\int_0^{2\pi}\left(\frac{\sigma_v}{a}-\frac{a}{\sigma_v}\right)\cos\psi_v\,\mathrm{d}\psi_v. \tag{4.12}$$

For small $(\sigma_v-a)/a$ we have an analytical form for $\sigma_v(\psi_v, T)$ (see (4.8)). This may be integrated analytically to give

$$F(T) = \frac{4\pi}{a}(b-a)\tanh T, \tag{4.13}$$

for small $(b-a)/a$ and moderate values of T.

The vortex deformations plotted in figure 3 show that, once the cylinder has moved enough to distort the vortex significantly, σ_v is close to a over much of the ring. Let us suppose that $\sigma_v \sim a$ for ψ_v in the ranges 0 to $\pi-\delta$ and $\pi+\delta$ to 2π. These regions do not contribute to the integral $F(T)$ and

$$F(T) \simeq \int_{\pi-\delta}^{\pi+\delta} -\cos\psi_v\left(\frac{\sigma_v}{a}-\frac{a}{\sigma_v}\right)\mathrm{d}\psi_v. \tag{4.14}$$

The integrand is zero at $\pi\mp\delta$. We also know the value of the integrand at $\psi_v = \pi$. It is $\sigma_{v\pi}(T)/a - a/\sigma_{v\pi}(T)$, where $\sigma_{v\pi}(T)$ is the solution of (4.10). A crude approximation to $F(T)$ can therefore be obtained by using Simpson's rule of integration to write

$$F(T) \simeq \frac{4\delta}{a}\left(\frac{\sigma_{v\pi}(T)}{a}-\frac{a}{\sigma_{v\pi}(T)}\right). \tag{4.15}$$

The value of δ can be found by applying Simpson's rule to the constant-area result in (4.7):

$$\pi(b^2-a^2) \simeq \frac{1}{2}\int_{\pi-\delta}^{\pi+\delta}(\sigma_v^2-a^2)\,\mathrm{d}\psi_v = \frac{2\delta}{3}(\sigma_{v\pi}^2(T)-a^2). \tag{4.16}$$

A combination of (4.15) and (4.16) leads to

$$F(T) \simeq \frac{2\pi(b^2-a^2)}{a\,\sigma_{v\pi}(T)}. \tag{4.17}$$

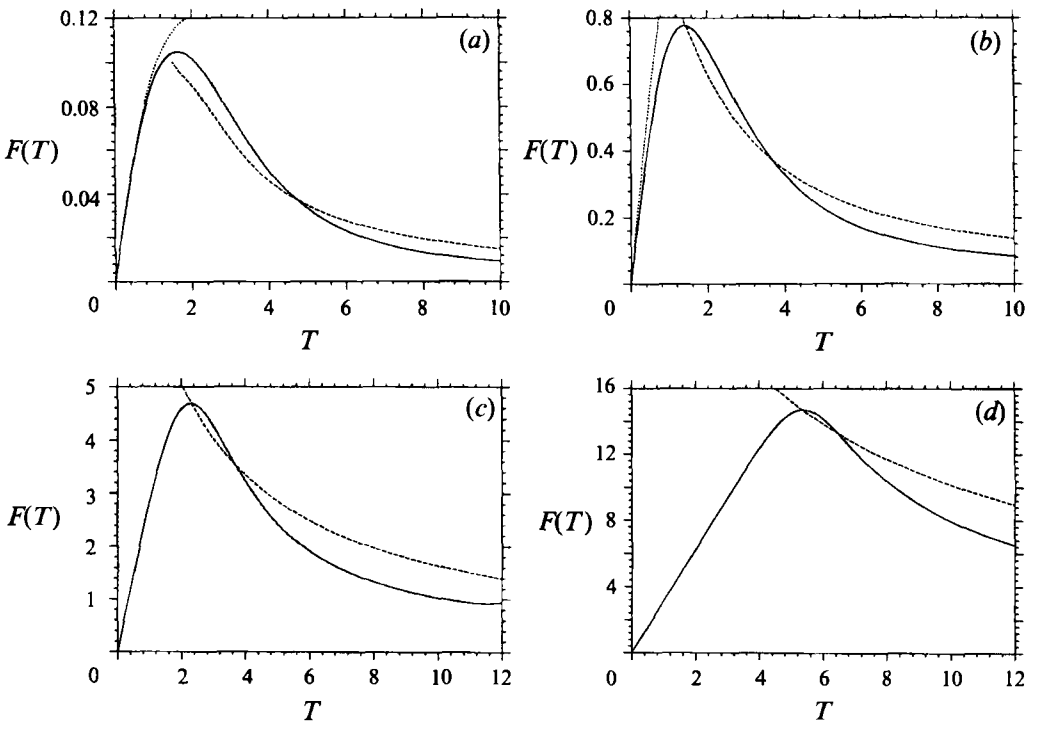

FIGURE 4. Evaluation of the function $F(T)$ as defined in (4.12) for (*a*) $b = 1.01a$, (*b*) $b = 1.1a$, (*c*) $b = 2a$, (*d*) $b = 5a$. ——, Numerical integration; ……, small-$(\sigma_v, -a)/a$ approximation (equation (4.13)); ------, Simpson's rule approximation (equation (4.17)).

This approximate form can only be expected to have limited validity. It requires T to be large enough for a significant distortion of the vortex ring. On the other hand, for very large values of T, the ring becomes so highly distorted near $\psi_v = \pi$ that the integral in (4.12) is no longer well approximated by our crude application of Simpson's rule.

The results in figure 4 show that $F(T)$ first increases linearly with T, reaches a maximum and then decays. For small $(b-a)/a$, the initial rise is well described by (4.13). In all cases the decay is reasonably well described by the Simpson's rule approximation in (4.17).

We have demonstrated that $F(T)$ is proportional to T for small T, and this may be used to infer the high-frequency asymptotic form of the pressure spectrum. For example, if $U_1(t)$ is constant, the Fourier transform of (4.11) leads to

$$\hat{p}_m(-k,\omega) = \mathrm{i}ka\rho\gamma_0 f(\omega + kU_1)/2\pi, \quad \text{where} \quad f(\omega) = \int_0^\infty U_T(t)\,F(T)\,\mathrm{e}^{-\mathrm{i}\omega t}\,\mathrm{d}t. \quad (4.18)$$

The form of $U_T(t)$ as $t \to 0$ will affect the high-frequency asymptotic form of $f(\omega)$. For example, suppose that the transverse motion is impulsive, so that U_T is a non-zero, positive constant for $t > 0$. Then T is proportional to t and $U_T(t)\,F(T) \propto t$ as $t \to 0^+$. Abel's theorem then gives $f(\omega) \propto \omega^{-2}$ as $|\omega| \to \infty$. If, on the other hand, the cylinder motion starts with a uniform acceleration, then $U_T(t)$ and T are proportional to t and t^2 respectively for small, positive t. Hence $U_T(t)\,F(T) \propto t^3$ as $t \to 0^+$ and it follows from Abel's theorem that $f(\omega) \propto \omega^{-4}$ as $|\omega| \to \infty$.

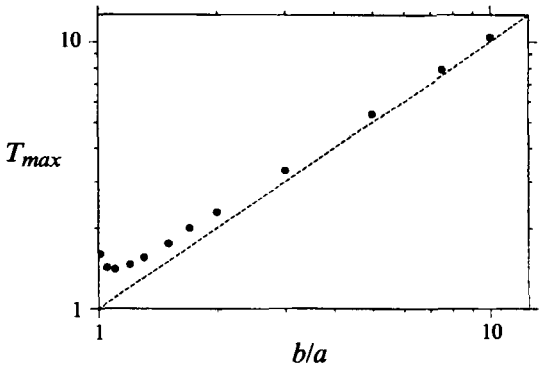

FIGURE 5. The variation of T_{max}, the value of T at which $F(T)$ has its maximum, with b/a: ●, results of numerical integration; ------, curve $T_{max} = b/a$.

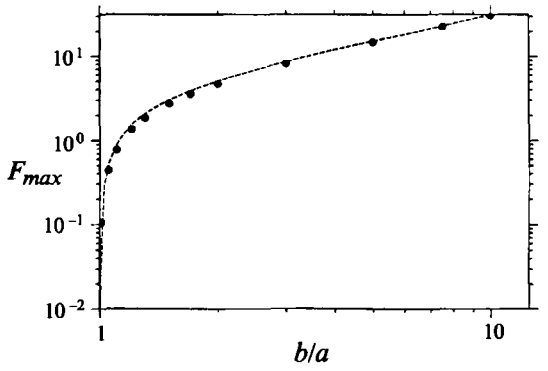

FIGURE 6. The variation of F_{max}, the maximum value of $F(T)$, with b/a: ●, results of numerical integration; ------, Simpson's rule approximation (equation (4.19)).

More information about the effect of the cylinder's manoeuvre on flow noise can be obtained by summarizing the information about the time history of $F(T)$ displayed in figure 4. These graphs suggest that the maximum values of F, F_{max} say, occur for values of T near b/a. This is confirmed in figure 5, which is a plot of T_{max}, the value of T at which F has its maximum for an initial vortex radius, against b/a. We see that (except for very small $(b-a)/a$) T_{max} does indeed lie close to b/a. This is not really surprising. Since T is the displacement of the cylinder non-dimensionalized with respect to a, at a time $T = b/a$ the cylinder has just reached the initial vortex position.

By the time $T = b/a$, the vortex has been significantly distorted and we can use (4.17), our Simpson's rule estimate of $F(b/a)$, to obtain an approximation to F_{max}. This procedure gives

$$F_{max} \simeq \frac{2\pi\,(b^2-a^2)}{a\,\sigma_{v\pi}(b/a)}, \tag{4.19}$$

where $\sigma_{v\pi}(b/a)$ is given by evaluating (4.10) for $T = b/a$.

This estimate of F_{max} is compared with the maximum found from numerical calculations in figure 6. The approximation works remarkably well. We see that a modest increase in b/a leads to a 100-fold increase in F_{max} and hence in the surface pressures. This variation is well described by the approximate form.

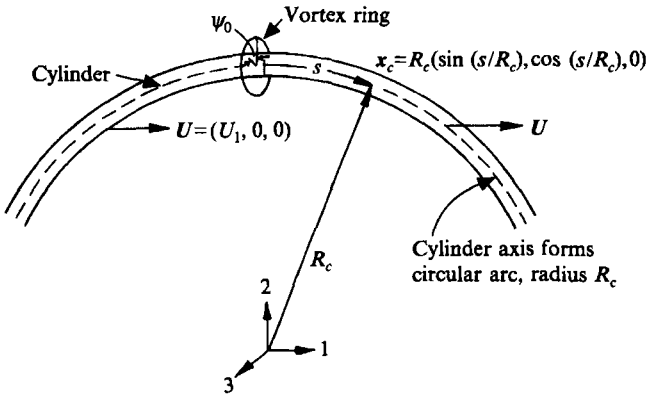

FIGURE 7. The cylinder and vortex ring at time $t = 0$.

In summary, the wavenumber decomposition of circumferentially averaged surface pressure is described by (4.11). The function $F(T)$ in this expression has been evaluated both approximately and numerically. These results show that F attains its maximum value at a time when the cylinder's manoeuvre takes it to the initial position of the vortex ring. The maximum value of F is strongly dependent on the initial radius of the vortex ring and this variation is well predicted by (4.19).

4.2. *A curved cylinder*

As an introductory example into the effects of curvature of the cylinder axis, consider a cylinder, whose axis forms part of a circular arc, in uniform motion. We investigate the particular case where

$$x_c(s,t) = R_c(\sin(s/R_c), \quad \cos(s/R_c), 0) + \int_0^t U(\tau)\,\mathrm{d}\tau \quad \text{and} \quad U = (U_1(t), 0, 0).$$

At $t = 0$, the vortex ring will be taken to be coaxial with the cylinder at $s = 0$ and of radius b. The geometry is illustrated in figure 7. We can anticipate the effects of cylinder motion on the vortex ring. Since vorticity moves with the fluid, the cylinder cannot cut through the ring. Hence, at times $t > 0$, as the curved cylinder moves through the ring, it must deflect the ring elements near $\psi_0 = \pi$ in the $-x_2$-direction and the ring is stretched.

A quantitative determination of ring distortion follows from an integration of (4.1). It is convenient to introduce variables $S_v(\psi_0, t)$ and $X_v(\psi_0, t)$ to describe the ring position at time t. $S_v(\psi_0, t)$ and $X_v(\psi_0, t)$ are related to $x_v(\psi_0, t)$ in the way indicated in (2.7) and (2.8). We expand $X_v(\psi_0, t)$, the perpendicular from the cylinder axis to $x_v(\psi_0, t)$, in polar coordinates $\sigma_v(\psi_0, t)$ and $\psi_v(\psi_0, t)$. Substitution for the velocity field from (2.27) into (4.1) leads, after extensive but straightforward algebra, to

$$\left.\frac{\partial S_v}{\partial t}\right|_{\psi_0} = -U_1(t)\cos(S_v/R_c)\left(1 + \frac{a\cos\psi_v}{R_c}\left(\frac{a}{\sigma_v} - \frac{\sigma_v}{a}\right)\right), \tag{4.20a}$$

$$\left.\frac{\partial \sigma_v}{\partial t}\right|_{\psi_0} = U_1(t)\sin(S_v/R_c)\cos\psi_v\left(-1 + \frac{a^2}{\sigma_v^2}\right), \tag{4.20b}$$

$$\left.\frac{\partial \psi_v}{\partial t}\right|_{\psi_0} = U_1(t)\sin(S_v/R_c)\sin\psi_v\left(1 + \frac{a^2}{\sigma_v^2} - \frac{a^2\cos\psi_v}{\sigma_v R_c}\right)\frac{1}{\sigma_v}. \tag{4.20c}$$

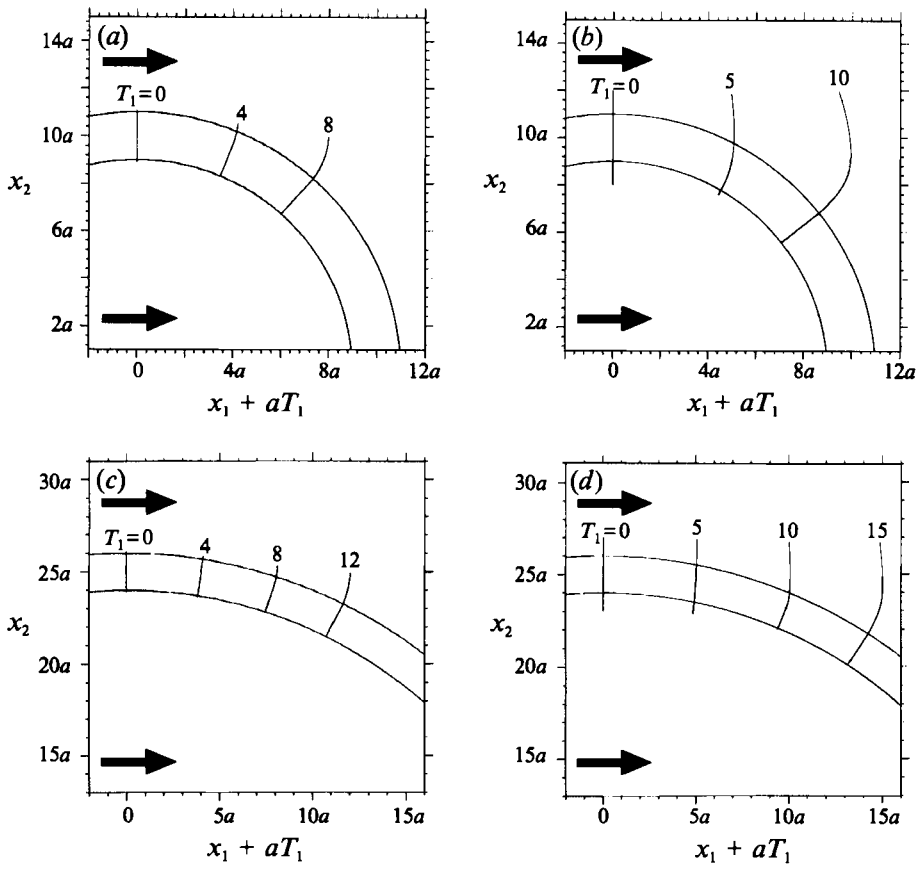

FIGURE 8. The projection of the vortex ring onto the (1, 2)-plane at various non-dimensional times: (*a*) $R_c = 10a$, $b = 1.1a$; (*b*) $R_c = 10a$, $b = 2.0a$; (*c*) $R_c = 25a$, $b = 1.1a$; (*d*) $R_c = 25a$, $b = 2.0a$.

The details of the algebraic manipulation are given in Dowling (1993). The right-hand sides of (4.20) clearly depend on the functional form of the axial cylinder velocity $U_1(t)$. However, this explicit dependence can be eliminated by introducing a new time-like variable

$$T_1 = -\int_0^t U_1(\tau)\,\mathrm{d}\tau/a.$$

We have included a minus sign in the definition of T_1 because we anticipate a motion in which $U_1(t)$ is negative. T_1 is the instantaneous displacement of the cylinder in the negative x_1-direction, non-dimensionalized with respect to the cylinder radius. Rewriting (4.20) in terms of T_1, we obtain

$$\frac{1}{a}\frac{\partial S_v}{\partial T_1}\bigg|_{\psi_0} = \cos(S_v/R_c)\left(1+\frac{a\cos\psi_v}{R_c}\left(\frac{a}{\sigma_v}-\frac{\sigma_v}{a}\right)\right), \tag{4.21a}$$

$$\frac{1}{a}\frac{\partial \sigma_v}{\partial T_1}\bigg|_{\psi_0} = \sin(S_v/R_c)\cos\psi_v\left(1-\frac{a^2}{\sigma_v^2}\right), \tag{4.21b}$$

$$\frac{\partial \psi_v}{\partial T_1}\bigg|_{\psi_0} = -\sin(S_v/R_c)\sin\psi_v\left(1+\frac{a^2}{\sigma_v^2}-\frac{a^2\cos\psi_v}{\sigma_v R_c}\right)\frac{a}{\sigma_v}. \tag{4.21c}$$

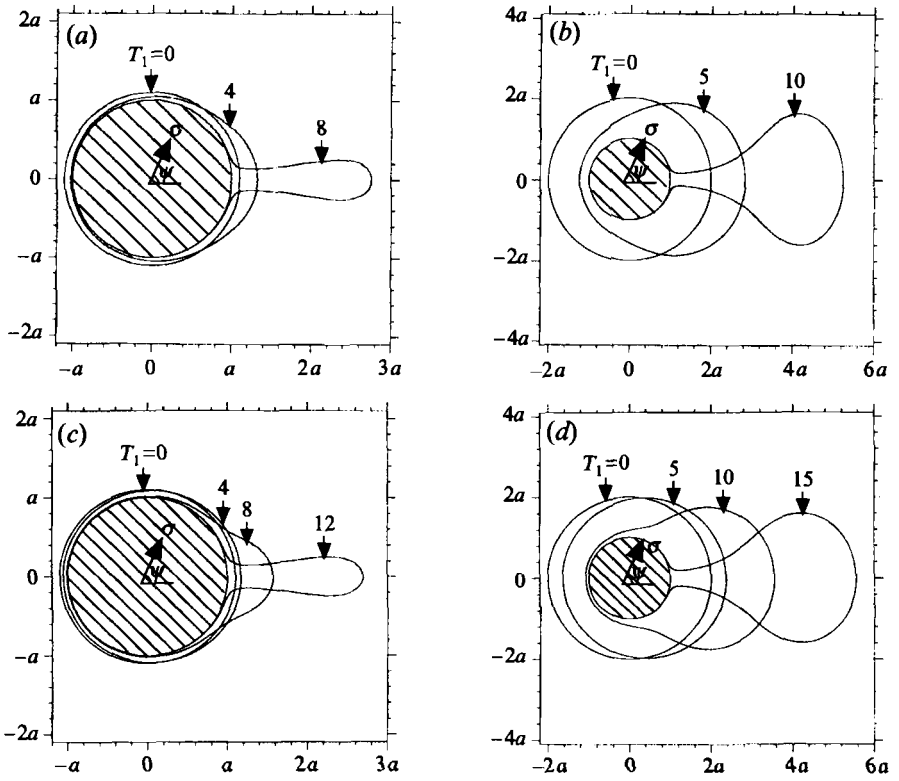

FIGURE 9. A polar plot of σ_v plotted as a function of ψ_v at various non-dimensional times: (*a*) $R_c = 10a$, $b = 1.1a$; (*b*) $R_c = 10a$, $b = 2.0a$; (*c*) $R_c = 25a$, $b = 1.1a$; (*d*) $R_c = 25a$, $b = 2.0a$.

The initial conditions are $S_v(\psi_0, 0) = 0$, $\sigma_v(\psi_0, 0) = b$ and $\psi_v(\psi_0, 0) = \psi_0$. It is a straightforward matter to integrate (4.21) numerically from these initial conditions to determine the subsequent shape of the vortex ring. Some results are shown in figures 8 and 9.

Since $a/\sigma_v - \sigma_v/a$ is negative, (4.21*a*) shows that S_v increases more rapidly for negative $\cos\psi_v$ than for positive $\cos\psi_v$. This means that elements of the vortex ring on the inside of the curve of the cylinder axis travel more rapidly along the cylinder than those on the outside and the ring tilts, as shown in figure 8. As the vortex ring is swept along the curved cylinder, the element of the ring near $\psi_0 = 0$ tends to remain at approximately the same x_2-position and the ring is stretched.

Figure 9 shows the distortion of the vortex ring perpendicular to the cylinder axis. The trends are similar to those induced by transverse motion of a straight cylinder in figure 3 and vorticity is essentially shed from the cylinder. We can explain these similarities directly from the equations of vortex motion.

Throughout the time that $(S_v/R_c)^2$ is small, (4.21*a*) can be integrated to show that $S_v = aT_1 + O(a\epsilon)$, where ϵ is order a/R_c. Hence, to lowest order in ϵ, equations (4.21*b*) and (4.21*c*) become

$$\frac{1}{a}\frac{\partial\sigma_v}{\partial T_1}\bigg|_{\psi_0} = \frac{aT_1}{R_c}\cos\psi_v\left(1-\frac{a^2}{\sigma_v^2}\right), \tag{4.22a}$$

$$\frac{\partial\psi_v}{\partial T_1}\bigg|_{\psi_0} = -\frac{aT_1}{R_c}\sin\psi_v\left(1+\frac{a^2}{\sigma_v^2}\right)\frac{a}{\sigma_v}. \tag{4.22b}$$

Equation (4.22) is identical to (4.6) provided we make the substitution $T = aT_1^2/2R_c$ and replace ψ_v by $\pi - \psi_v$. The integration of (4.6) showed that the vortex ring is shed from the straight cylinder by the non-dimensional time $T = b/a$. Therefore, by analogy, we can expect the vorticity to be shed from the curved cylinder by $T_1 = (2bR_c)^{1/2}/a$, and this is confirmed by the plots of vortex ring geometry in figure 9.

The results in figures 3, 8 and 9 can be combined into the statement that transverse displacement of the cylinder axis causes distortion of boundary-layer vorticity. The vorticity is essentially shed from the cylinder once the cylinder's transverse displacement exceeds the boundary-layer thickness. The effect on the vorticity is similar however the cylinder's transverse displacement is produced.

The vortex ring travels an axial distance of order $(2bR_c)^{1/2}$ before it is shed from the cylinder. It is therefore important to retain terms of order a/R_c in (4.21), when describing the convection of the vorticity. Small errors in velocity lead to significant errors in the position of the vorticity after it has been convected this distance. However, once the instantaneous position of the vorticity is known, surface pressures induced on the cylinder near the vorticity can be deduced by treating the cylinder as locally straight, with an error of only order ϵ in comparison with unity. Before we can use the result in (4.3) for the wavenumber decomposition of the circumferentially averaged surface pressure we must introduce local cylindrical polar coordinates aligned with the cylinder axis near the vorticity.

At a non-dimensional time T_1, the cylinder has moved a distance aT_1 in the negative 1-direction. The vortex ring is then near arclength $S_0(T_1)$ of the cylinder where from (4.21*a*)

$$\frac{1}{a}\frac{\mathrm{d}S_0}{\mathrm{d}T_1} = \cos(S_0/R_c). \tag{4.23}$$

This integrates to give

$$\sin\left(\frac{S_0(T_1)}{R_c}\right) = \frac{\mathrm{e}^{2aT_1/R_c} - 1}{\mathrm{e}^{2aT_1/R_c} + 1}. \tag{4.24}$$

Write $\boldsymbol{x}_v' = \boldsymbol{x}_v + aT_1\boldsymbol{e}_1 - \boldsymbol{x}_c(S_0(T_1), T_1)$ in local cylindrical polar coordinates: $\boldsymbol{x}_v' = (S_v - S_0(T_1), \sigma_v, \psi_v)$. In this coordinate system $U_{\sigma_v} = U_1 \sin(S_0/R_c)\cos\psi_v$ and $U_{\psi_v} = -U_1 \sin(S_0/R_c)\sin\psi_v$. Substitution into (4.3) leads to

$$p_m(-k, T_1) = \frac{\rho\gamma_0 U_1 \sin(S_0/R_c)}{2\pi}\int_0^{2\pi}\left(\frac{\partial S_v}{\partial\psi_0}\sin\psi_v - \mathrm{i}k\sigma_v^2\frac{\partial\psi_v}{\partial\psi_0}\cos\psi_v\right) \times\left(\frac{1}{\sigma_v} - \frac{a^2}{\sigma_v^3}\right)\mathrm{e}^{\mathrm{i}k(S_v - S_0(T_1))}\,\mathrm{d}\psi_0. \tag{4.25}$$

For small $k(S_v - S_0(T_1))$, the exponential may be expanded to give

$$p_m(-k, T_1) = \frac{\rho\gamma_0 U_1}{2\pi}[A(T_1) + \mathrm{i}ka\,B(T_1)], \tag{4.26}$$

where

$$A(T_1) = \sin(S_0/R_c)\int_0^{2\pi}\frac{\partial S_v}{\partial\psi_0}\sin\psi_v\left(\frac{1}{\sigma_v} - \frac{a^2}{\sigma_v^3}\right)\mathrm{d}\psi_0, \tag{4.27}$$

$$B(T_1) = \frac{\sin(S_0/R_c)}{a}\int_0^{2\pi}\left((S_v - S_0(t))\frac{\partial S_v}{\partial\psi_0}\sin\psi_v - \sigma_v^2\frac{\partial\psi_v}{\partial\psi_0}\cos\psi_v\right)\left(\frac{1}{\sigma_v} - \frac{a^2}{\sigma_v^3}\right)\mathrm{d}\psi_0; \tag{4.28}$$

$p_m(-k, T_1)$ described by (4.26) is a local Fourier transform obtained by an integration over S centred on $S_0(T_1)$:

$$p_m(-k, T_1) = \frac{1}{2\pi}\int (p-p_\infty)(x, T_1)\, e^{ik(S-S_0(T_1))}\, d\theta\, dS = p_s(-k, T_1)\, e^{-ikS_0(T_1)}, \quad (4.29)$$

where $p_s(-k, T_1)$ is the Fourier transform of the circumferentially averaged pressure with respect to arclength S. From a combination of (4.26) and (4.29)

$$p_s(-k, T_1) = \frac{\rho\gamma_0 U_1}{2\pi} e^{ikS_0(T_1)}[A(T_1) + ikaB(T_1)]. \quad (4.30)$$

The functions $A(T_1)$ and $B(T_1)$ are plotted in figure 10 for different values of b/a and R_c/a. It is evident from the figure that A is very small in comparison with $|B|$. This is partly because S_v varies only slowly with ψ_0, and partly because the maximum values of $|\partial S_v/\partial\psi_0|$ occur where $\sin\psi_v$ is small. For similar reasons the first term in the integral defining $B(T_1)$ is much smaller than the second.

We can deduce from the relative magnitudes of $A(T_1)$ and $B(T_1)$ shown in figure 10 that, over most of the range $|k|R_c \gg 1$, the main contribution to the surface pressure decomposition in (4.30) is

$$p_s(-k, t) = \frac{ika\rho\gamma_0}{2\pi} \exp(ikS_0(T_1))\, U_1(t)\, B(T_1). \quad (4.31)$$

The expression for $p_m(-k, t)$ described in (4.31) for the curved cylinder is similar to that for the straight cylinder in (4.11). Once again the cross-power spectral density for the surface pressure is predicted to be proportional to k^2. The similarity between the two forms can be highlighted by introducing new variables.

We will use l as an independent variable where, $al(T_1) = R_c - R_c\cos(S_0(T_1)/R_c)$, is the transverse displacement of the cylinder axis at $S_0(T_1)$. With the new dependent variable, $F_1(l) = B(T_1)/\sin(S_0/R_c)$, equation (4.31) leads to

$$p_s(-k, t) = \frac{ika\rho\gamma_0}{2\pi} \exp(ikS_0(T_1))\, U_1(t) \sin(S_0/R_c)\, F_1(l). \quad (4.32)$$

We note that in this example $U_1(t)\sin(S_0/R_c)$ is the cylinder velocity transverse to its local axis. $U_1(t)\sin(S_0/R_c)$ in (4.32) is therefore directly comparable with the variable $U_T(t)$ in (4.11).

$F_1(l)$ is plotted in figure 11 and is found to have a form virtually independent of the radius of curvature of the cylinder centreline. The peak pressure fluctuations are generated when l is approximately equal to b/a. This is when the transverse cylinder displacement is equal to the initial radius of the vortex ring, a result that is reminiscent of that for the straight cylinder (see figure 5). The function $-F(T)$ for the straight cylinder, which was plotted in figure 4, is also shown on figure 11 for comparison. It is clear that $-F(T)$ is a good approximation to $F_1(l)$ for different values of R_c and b. Therefore the results in §4.1 describing the variation of $F(T)$ can also be applied to $F_1(l)$.

In summary, we have considered two particular examples in some detail. In the first, the transverse cylinder displacement is produced by transverse motion of a straight cylinder. In the second, the cylinder axis near the vortex ring is displaced laterally by the longitudinal velocity of a cylinder with a curved axis. In both cases the wavenumber decomposition of the circumferentially averaged pressure spectrum is proportional to k^2. Moreover the magnitude of the pressure is proportional to the product of the transverse cylinder velocity at the position of the vortex and a function F. The function F depends on the transverse displacement of the cylinder, and attains its maximum at

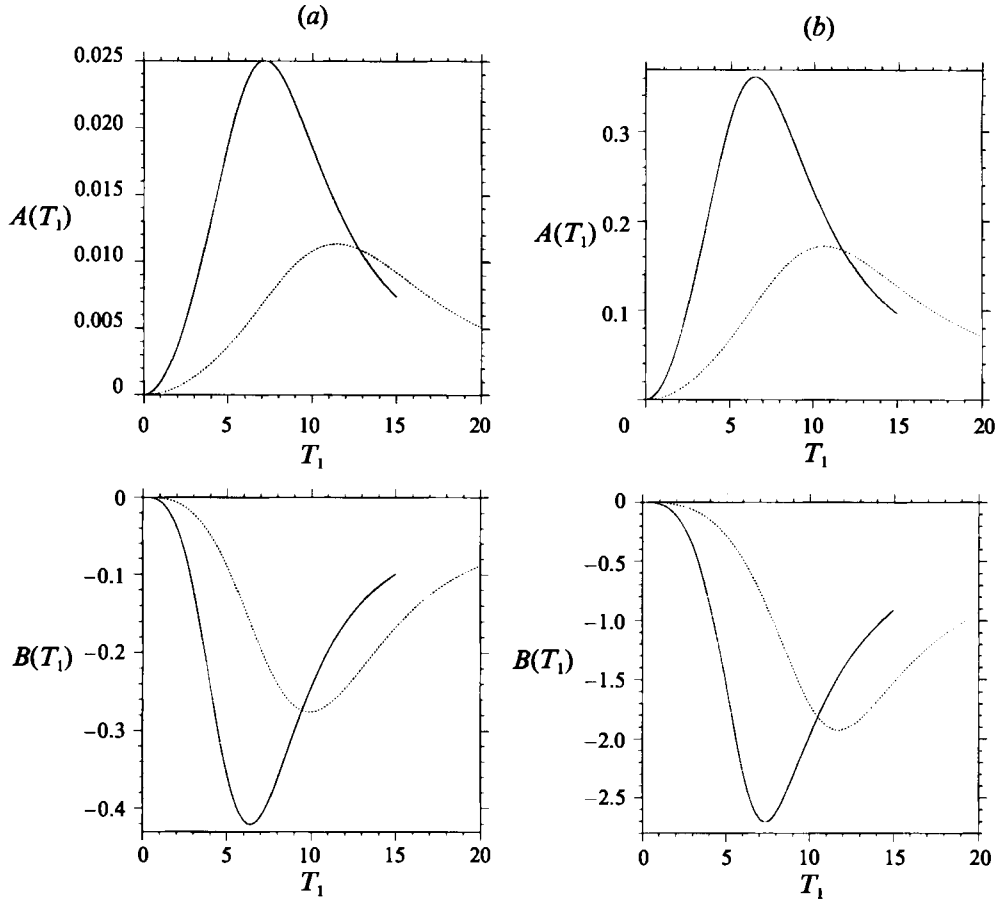

FIGURE 10. Evaluation of the functions $A(T_1)$ and $B(T_1)$ as defined in (4.27) and (4.28) for (*a*) $b = 1.1a$, (*b*) $b = 2.0a$. ——, $R_c = 10a$; . . . . . , $R_c = 25a$.

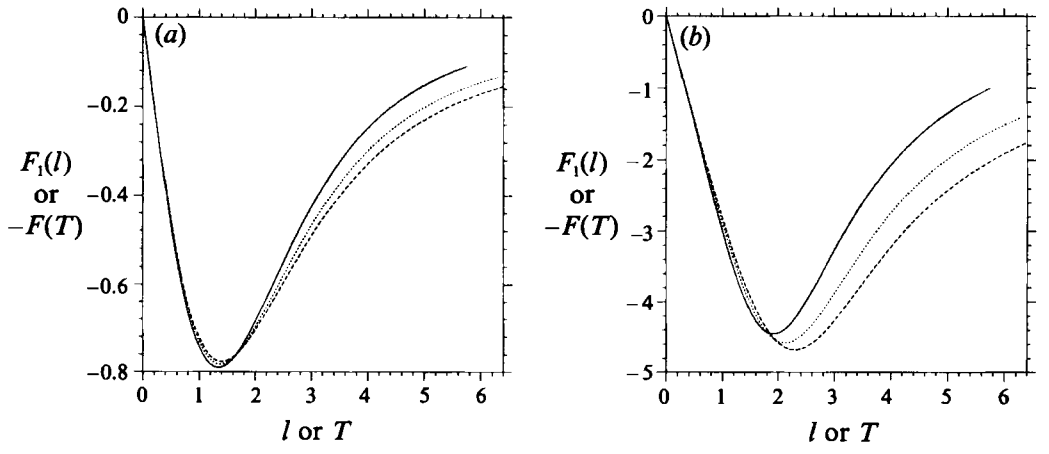

FIGURE 11. The variation of F_1 with non-dimensional displacement l for (*a*) $b = 1.1a$, (*b*) $b = 2.0a$. ——, F_1 (l), $R_c = 10a$; . . . . . , F_1 (l), $R_c = 25a$; ------, $-F(T)$.

a time when the cylinder's manoeuvre takes it to the initial position of the vortex ring. The maximum value of F is strongly dependent on the initial radius of the vortex ring in the way described by (4.19) and illustrated in figure 6.

5. Conclusions

The velocity field due to a moving cylinder has been decomposed into an irrotational component and an additional term due to vorticity. The irrotational flow produced by an arbitrary unsteady motion of a cylinder with a slightly curved axis was determined in §2 (see (2.27)). The effect of vorticity was considered in §3, where a vector Green function was used to derive a general representation for the velocity potential outside the regions of vorticity, in terms of a weighted integral over the vorticity distribution. Having determined an expression for the velocity potential it is straightforward to calculate other flow parameters, like velocity and pressure. We use it to derive an expression for $p_m(k, t)$, the axial wavenumber decomposition of the circumferentially averaged surface pressure induced by an arbitrary distribution of vorticity near the moving cylinder. The general form is given in (3.30). This simplifies to the expression in (3.32) when the vorticity is weak and convects with the irrotational fluid velocity induced by the cylinder motion. Equation (3.32) describes the wavenumber decomposition of the circumferentially averaged pressure in terms of a weighted volume integral over the instantaneous vorticity field. Two things are striking about its form. First, it shows that the pressure spectrum is proportional to $(ka)^2$ in a boundary layer in which the vorticity is primarily azimuthal, but that there is an additional term independent of wavenumber when there is significant axial vorticity. Secondly, it demonstrates that as parts of the vorticity approach the cylinder they do not contribute to $p_m(k, t)$.

An application of this representation theorem is described in §4, where the unsteady pressures generated when a cylinder with an established boundary layer undergoes lateral displacement were investigated. The model of an element of boundary-layer vorticity was highly simplified. Nevertheless, our results were found not to depend on the details of the lateral displacement which leads us to believe that they have wider applicability. These results suggest that transverse cylinder motion causes boundary-layer vorticity to be shed from a cylinder once the displacement of the axis of the cylinder exceeds the boundary-layer thickness. Hence along the flexible cylinder the boundary layer will repeatedly grow and then be shed.

The circumferentially averaged pressure spectrum generated by the shedding of a vortex ring was found to be proportional to the square of the axial wavenumber. The magnitude of the pressure depends on the product of the transverse velocity of the cylinder with a function F (see (4.11)). F is a function of the transverse displacement of the cylinder, and attains its maximum at a time when the cylinder's manoeuvre takes it to the initial position of the vortex ring. The maximum value of F is strongly dependent on the initial radius of the vortex ring in the way described by (4.19) and illustrated in figure 6. F_{max} increases significantly as the initial radius of the ring increases.

A cylindrically symmetric boundary layer may be considered as a superposition of vortex rings, whose strengths are a function of their radius and axial position. Then, for a specified initial distribution of vorticity and transverse velocity, (4.11) and figures 4 and 6 can be used to infer the form of the surface pressure spectrum induced as this established boundary layer is shed by the lateral motion of the cylinder. In particular, it is evident from figure 4 that the surface pressures due to this vortex shedding are not

significant once the lateral displacement of the cylinder exceeds about twice the initial boundary-layer thickness.

This work has been carried out with the support of the Defence Research Agency and Topexpress Ltd.

Appendix A. The velocity field induced by vorticity near a moving cylinder

The velocity field satisfies

$$\text{curl } \boldsymbol{v} = \boldsymbol{\omega}, \tag{A 1}$$

with

$$\boldsymbol{n}\cdot\nabla\boldsymbol{v} = \boldsymbol{n}\cdot\boldsymbol{U} \quad \text{on the cylinder.} \tag{A 2}$$

In free space (Batchelor 1967, p. 87), the solution to (A 1) is

$$\boldsymbol{v}_f(\boldsymbol{x},t) = -\int \frac{(\boldsymbol{x}-\boldsymbol{y})\times\boldsymbol{\omega}(\boldsymbol{y},t)}{4\pi|\boldsymbol{x}-\boldsymbol{y}|^3}\,\mathrm{d}^3\boldsymbol{y}. \tag{A 3}$$

This velocity field is a particular integral of (A 1). In order to find the solution that satisfies the boundary condition (A 2) we add on an irrotational velocity field and write

$$\boldsymbol{v}(\boldsymbol{x},t) = \boldsymbol{v}_f(\boldsymbol{x},t) + \nabla\phi_c. \tag{A 4}$$

The continuity equation then leads to

$$\nabla^2\phi_c = 0, \tag{A 5}$$

and it follows from the boundary condition (A 2) that

$$\boldsymbol{n}\cdot\nabla\phi_c = \boldsymbol{n}\cdot\boldsymbol{U} + \int \frac{\boldsymbol{n}\cdot(\boldsymbol{x}-\boldsymbol{y})\times\boldsymbol{\omega}(\boldsymbol{y},t)}{4\pi|\boldsymbol{x}-\boldsymbol{y}|^3}\,\mathrm{d}^3\boldsymbol{y}. \tag{A 6}$$

For a curved cylinder in arbitrary motion the solution to Laplace's equation which satisfies the boundary condition $\boldsymbol{n}\cdot\nabla\phi = \boldsymbol{n}\cdot\boldsymbol{U}$ is given correct to order ϵ by (2.26). The additional contribution to ϕ_c to account for the effect of the vorticity in the boundary condition (A 6) could be calculated easily numerically by, for example, a panel method. This determines the instantaneous velocity field in terms of the cylinder velocity and three-dimensional vorticity. Equation (3.6) could then be integrated with respect to time to find the development of the vorticity field.

The curvature of the cylinder axis leads to small terms of order ϵ in the fluid velocity. Over a large time interval, the integrated effect of this small velocity change may be significant. Hence the development of the vorticity field over an appreciable time interval may be influenced by the curvature of the cylinder axis. However, in (3.29) and (3.30) the instantaneous velocity field is only required to zeroth order in ϵ. Then the cylinder may be considered as straight with a uniform velocity $\boldsymbol{U}(t)$ and an analytical solution for $\boldsymbol{v}$ can be determined.

It is convenient to use a reference frame which moves with the cylinder,

$$\boldsymbol{x}' = \boldsymbol{x} - \int_0^t \boldsymbol{U}(\tau)\,\mathrm{d}t, \quad \boldsymbol{y}' = \boldsymbol{y} - \int_0^t \boldsymbol{U}(\tau)\,\mathrm{d}t \quad \text{and} \quad \boldsymbol{v}' = \boldsymbol{v} - \boldsymbol{U}(t).$$

Introduce cylindrical polar coordinates $\boldsymbol{x}' = (x_1', R, \theta)$, $\boldsymbol{y}' = (y_1', \sigma, \psi)$, the 1-direction being taken parallel to the local cylinder axis.

Then $\boldsymbol{v}' = \boldsymbol{v}_f + \nabla\phi_c'$ and it follows from (A 2) that

$$\left.\frac{\partial\phi_c'}{\partial R}\right|_{R=a} = \int [\cos(\theta-\psi)((\boldsymbol{x}'-\boldsymbol{y}')\times\boldsymbol{\omega})_\sigma + \sin(\theta-\psi)((\boldsymbol{x}'-\boldsymbol{y}')\times\boldsymbol{\omega})_\psi]\frac{\mathrm{d}^3\boldsymbol{y}'}{4\pi|\boldsymbol{x}'-\boldsymbol{y}'|^3}. \tag{A 7}$$

In cylindrical polar coordinates $(x'-y')/|x'-y'|^3$ can be expanded in harmonics to show that for x on the cylinder

$$\frac{x'-y'}{|x'-y'|^3} = \frac{1}{\pi}\sum_{n=-\infty}^{\infty}\int\left(ikK_n(\kappa\sigma), \kappa\dot{K}_n(\kappa\sigma), \frac{in}{\sigma}K_n(\kappa\sigma)\right) I_n(\kappa a)\, e^{ik(y_1'-x_1')+in(\psi-\theta)}\, dk$$

for $a < \sigma$, (A 8)

where $\kappa = |k|$. $I_n(z)$ and $K_n(z)$ are modified Bessel functions and a dot denotes differentiation with respect to the argument. The boundary condition (A 7) can therefore be rewritten as

$$\left.\frac{\partial\phi_c'}{\partial R}\right|_{R=a} = \sum_{n=-\infty}^{\infty}\int A_n(k)\, e^{-ikx_1'-in\theta}\, dk, \tag{A 9}$$

where

$$\begin{aligned}8\pi^2 A_n(k) = \int\Big[&\left(\omega_1\left(\frac{i(n-1)}{\sigma}K_{n-1}(\kappa\sigma) - i\kappa\dot{K}_{n-1}(\kappa\sigma)\right) - \omega_\sigma kK_{n-1}(\kappa\sigma) - \omega_\psi ikK_{n-1}(\kappa\sigma)\right) I_{n-1}(\kappa a)\\ &+\left(\omega_1\left(\frac{i(n+1)}{\sigma}K_{n+1}(\kappa\sigma) + i\kappa\dot{K}_{n+1}(\kappa\sigma)\right)\right.\\ &\left.+\omega_\sigma kK_{n+1}(\kappa\sigma) - \omega_\psi ikK_{n+1}(\kappa\sigma)\right) I_{n+1}(\kappa a)\Big] e^{iky_1'+in\psi}\, d^3y'.\end{aligned} \tag{A 10}$$

The solution to $\nabla^2\phi_c' = 0$ that satisfies the boundary condition (A 9) and tends to $-U\cdot x'$ at infinity is

$$\phi_c'(x,t) = \sum_{n=-\infty}^{\infty}\int\frac{A_n(k)}{\kappa\dot{K}_n(\kappa a)}K_n(\kappa R)\, e^{-ikx_1'-in\theta}\, dk - U\cdot x' - (U_2\cos\theta + U_3\sin\theta)a^2/R. \tag{A 11}$$

The velocity field then follows:

$$\begin{aligned}v' = v_f + \nabla\phi_c' = &-\int\frac{(x'-y')\times\omega(y',t)}{4\pi|x'-y'|^3}\, d^3y'\\ &+\sum_{n=-\infty}^{\infty}\int\frac{A_n(k)}{\kappa\dot{K}_n(\kappa a)}\left(-ikK_n(\kappa R), \kappa\dot{K}_n(kR), -\frac{in}{R}K_n(\kappa R)\right) e^{-ikx_1'-in\theta}\, dk\\ &-U+(0, U_2\cos\theta + U_3\sin\theta, U_2\sin\theta - U_3\cos\theta)a^2/R^2 + O(\epsilon).\end{aligned} \tag{A 12}$$

$A_n(k)$ is given by (A 10) as an integral over the instantaneous vorticity field. Equation (A 12) is therefore a representation of the velocity field induced by an arbitrary distribution of vorticity near a moving cylinder. The first term on the right-hand side describes the velocity field that would be generated by the vorticity in unbounded space, while the second term accounts for the scattering effect of the cylinder. The remaining terms are those induced directly by the cylinder velocity.

Appendix B. Evaluation of the vector Green function

$G(y', |x')$ is the solution of Laplace's equation with a point source at x' that satisfies $n\cdot\nabla G = 0$ on the surface of the cylinder (see (3.16)). It is convenient to expand $x' = (x_1', R, \theta)$, $y' = (y_1', \sigma, \psi)$ in cylindrical polar coordinates, with the 1-direction being taken parallel to the local cylinder axis. The method of solution for $G(y'|x')$ is

standard and is described, for example, in Morse & Feshbach (1953, chapter 10). For $R \leqslant \sigma$, this leads to

$$G(y' \mid x') = \sum_{n=-\infty}^{\infty} \int C(n, \kappa, x)\, K_n(\kappa\sigma)\, \mathrm{e}^{\mathrm{i}ky_1' + \mathrm{i}n\psi}\, \mathrm{d}k \quad \text{for} \quad R < \sigma, \tag{B 1}$$

where

$$C(n, k, x) = -\frac{1}{(2\pi)^2}\left(I_n(\kappa R) - \frac{\dot{I}_n(\kappa a)}{\dot{K}_n(\kappa a)} K_n(\kappa R)\right) \mathrm{e}^{-\mathrm{i}kx_1' - \mathrm{i}n\theta} \tag{B 2}$$

and $\kappa = |k|$.

The vector Green function $G(y' \mid x')$ is defined by (3.18):

$$\operatorname{curl} G = \operatorname{grad} G. \tag{B 3}$$

This equation only determines G to within the addition of any irrotational function and we can use this arbitrariness to choose the radial component of G to be zero. Then, after substitution for G from (B 1), equation (B 3) simplifies to

$$\frac{\partial G_1}{\partial \sigma} = -\frac{1}{\sigma} \sum_{n=-\infty}^{\infty} \int C(n, k, x)\, \mathrm{i}nK_n(\kappa\sigma)\, \mathrm{e}^{\mathrm{i}ky_1' + \mathrm{i}n\psi}\, \mathrm{d}k, \tag{B 4a}$$

$$\frac{\partial}{\partial \sigma}(\sigma G_\psi) = \sigma \sum_{n=-\infty}^{\infty} C(n, k, x)\, \mathrm{i}kK_n(\kappa\sigma)\, \mathrm{e}^{\mathrm{i}ky_1' + \mathrm{i}n\psi}\, \mathrm{d}k. \tag{B 4b}$$

After integration, we obtain

$$G = \sum_{n=-\infty}^{\infty} \int C(n, k, x)\left(\mathrm{i}n \int_{\kappa\sigma}^{\infty} \frac{K_n(z)\, \mathrm{d}z}{z}, 0, -\frac{\mathrm{i}}{k\sigma} \int_{\kappa\sigma}^{\infty} zK_n(z)\, \mathrm{d}z\right) \mathrm{e}^{\mathrm{i}ky_1' + \mathrm{i}n\psi}\, \mathrm{d}k. \tag{B 5}$$

Substitution for $C(n, k, x)$ from (B 2) leads to

$$G = \frac{\mathrm{i}a}{(2\pi)^2} \sum_{n=-\infty}^{\infty} \int \left(-nQ_n, 0, \frac{P_n}{k\sigma}\right) \kappa(I_n(\kappa R)\, \dot{K}_n(\kappa a) - \dot{I}_n(\kappa a)\, K_n(\kappa R))\, \mathrm{e}^{\mathrm{i}k(y_1' - x_1') + \mathrm{i}n(\psi - \theta)}\, \mathrm{d}k, \tag{B 6}$$

where

$$P_n = \frac{1}{\kappa a \dot{K}_n(\kappa a)} \int_{\kappa\sigma}^{\infty} zK_n(z)\, \mathrm{d}z \quad \text{and} \quad Q_n = \frac{1}{\kappa a \dot{K}_n(\kappa a)} \int_{\kappa\sigma}^{\infty} \frac{K_n(z)}{z}\, \mathrm{d}z,$$

a result that is used in (3.23).

Appendix C. Simplification of the wavenumber decomposition of the circumferentially averaged pressure

The condition

$$\operatorname{div} \omega = 0 = \frac{\partial \omega_1}{\partial y_1'} + \frac{1}{\sigma}\frac{\partial}{\partial \sigma}(\sigma\omega_\sigma) + \frac{1}{\sigma}\frac{\partial \omega_\psi}{\partial \psi} \tag{C 1}$$

implies a relationship between the three components of vorticity, which may be exploited to simplify the expression for $p_m(-k, t)$ in (3.31).

We begin by introducing a function $S(y, k)$ defined by

$$\frac{\partial S}{\partial \sigma} = \left(1 + \frac{a^2}{\sigma^2}\right)(\ln(\tfrac{1}{2}k\sigma) + \gamma)\, U_\psi. \tag{C 2}$$

Integration shows that

$$S(y,k) = \left(\sigma - \frac{a^2}{\sigma}\right)(\ln(\tfrac{1}{2}k\sigma) + \gamma)\, U_\psi - \left(\sigma + \frac{a^2}{\sigma}\right) U_\psi + s_0(y_1', \psi), \tag{C 3}$$

where $s_0(y_1', \psi)$ may be chosen arbitrarily.

The integral describing $p_m(-k,t)$ in (3.31) contains a term

$$I = -\frac{\rho i k}{2\pi} \int \omega_\sigma \frac{\partial S}{\partial \sigma} e^{iky_1'} \, d^3y'. \tag{C 4}$$

After integration by parts and use of (C 1) we obtain

$$I = -\frac{\rho i k}{2\pi} \int \left(\frac{\partial \omega_1}{\partial y_1'} + \frac{1}{\sigma}\frac{\partial \omega_\psi}{\partial \psi}\right) S\, e^{iky_1'} \, d^3y' \tag{C 5}$$

$$= \frac{\rho i k}{2\pi} \int \left(\omega_1 \sigma \frac{\partial}{\partial y_1'}(S\, e^{iky_1'}) + \omega_\psi \frac{\partial}{\partial \psi}(S\, e^{iky_1'})\right) \frac{d^3y'}{\sigma} \tag{C 6}$$

after a further integration by parts.

When $s_0(y_1', \psi)$ is chosen to be $\pi U_\psi / k$ and (C 6) is substituted into (3.31), the expression for $p_m(-k,t)$ simplifies to the form in (3.32), if terms of order $(ka)^2$ are neglected in comparison with unity.

REFERENCES

BATCHELOR, G. K. 1967 *An Introduction to Fluid Dynamics*. Cambridge University Press.

CHASE, D. M. & NOISEUX, C. F. 1982 Turbulent wall pressure at low wavenumbers: relation to nonlinear sources in planar and cylindrical flow. *J. Acoust. Soc. Am.* **7**, 975–982.

DHANAK, M. R. 1988 Turbulent boundary layer on circular cylinder: the low-wavenumber surface pressure spectrum due to a low-Mach number flow. *J. Fluid Mech.* **191**, 443–464.

DOWLING, A. P. 1988 The dynamics of towed flexible cylinders. Part 1. Neutrally buoyant elements. *J. Fluid Mech.* **187**, 507–532.

DOWLING, A. P. 1993 Vortex sound near a moving cylinder. *Cambridge University Engineering Department, Tech. Rep.* CUED/A/TR20.

KENNEDY, R. M. 1980 Transverse motion response of a cable-towed system. Part 1. Theory. *US J. Underwater Acoust.* **30**, 97–108.

LIGHTHILL, M. J. 1956 The image system of a vortex element in a rigid sphere. *Proc. Camb. Phil. Soc.* **52**, 317–321.

LIGHTHILL, M. J. 1960 Note on the swimming of slender fish. *J. Fluid Mech.* **9**, 305–317.

MÖHRING, W. 1978 On vortex sound at low Mach number. *J. Fluid Mech.* **85**, 685–691.

MORSE, P. M. & FESHBACH, H. 1953 *Methods of Theoretical Physics*. McGraw-Hill.

PAIDOUSSIS, M. P. 1973 Dynamics of cylindrical structures subjected to axial flow. *J. Sound Vib.* **29**, 365–385.

TAYLOR, G. I. 1952 Analysis of the swimming of long and narrow animals. *Proc. R. Soc. Lond.* A **214**, 158–183.